Effects of moderate Reynolds numbers on subsonic round jets with highly disturbed nozzle-exit boundary layers

Christophe Bogey, Olivier Marsden, and Christophe Bailly

Related Articles

Additional information on Phys. Fluids

Effects of moderate Reynolds numbers on subsonic round jets with highly disturbed nozzle-exit boundary layers

Christophe Bogey,[1,a)] Olivier Marsden,[1] and Christophe Bailly[1,2]
[1]*Laboratoire de Mécanique des Fluides et d'Acoustique, UMR CNRS 5509,
Ecole Centrale de Lyon, Université de Lyon, 69134 Ecully Cedex, France*
[2]*Institut Universitaire de France, 103 boulevard Saint-Michel, 75005 Paris, France*

The effects of moderate Reynolds numbers on the flow and acoustic fields of initially highly disturbed isothermal round jets at Mach number $M = 0.9$ and diameter-based Reynolds numbers Re_D between 2.5×10^4 and 2×10^5 are investigated using large-eddy simulation under carefully controlled conditions. To the best of our knowledge, this is the first comprehensive study of its kind. The jets originate at $z = 0$ from a pipe nozzle of radius r_0, in which a tripping procedure is applied to the boundary layers. At the nozzle exit, laminar-like mean velocity profiles of thickness $\delta \simeq 0.15 r_0$ and momentum thickness $\delta_\theta \simeq 0.018 r_0$, yielding Reynolds numbers Re_θ varying from 256 to 1856 depending on Re_D, and peak turbulence intensities around 9% of the jet velocity, are thus obtained. As the Reynolds number increases, the mixing layers develop more slowly, with smaller integral length scales and lower levels of velocity fluctuations. The axial profiles of turbulence intensities become smoother, showing a clear overshoot around $z = 2 r_0$ at $Re_D = 2.5 \times 10^4$, but a monotonical growth at $Re_D = 2 \times 10^5$. Velocity spectra downstream of the nozzle exit also broaden with Re_D, as expected. Large-scale components usually observed in turbulent boundary layers and shear layers, characterized by Strouhal numbers $St_\theta \simeq 0.013$ around $z = r_0$ and by azimuthal spacings $\lambda_\theta \simeq \delta$, remain dominant, although the contribution of fine-scale structures with $\lambda_\theta \leq \delta/2$ strengthens. Moreover, with rising Re_D, the jet potential core lengthens slightly, but the flow properties do not change significantly farther downstream. Finally, lower sound pressure levels are generated, with a decrease of about 2 dB over the range of Re_D considered. © *2012 American Institute of Physics.* [http://dx.doi.org/10.1063/1.4757667]

I. INTRODUCTION

For at least fifty years, and since pioneering works such as those by Sato[1] and Mollö-Christensen and Narasimha,[2] the Reynolds number has been recognized as an important parameter in jets as far as both flow development and sound emission are concerned. In round jets in particular, while turbulent features are classically expected to be independent of the Reynolds number provided it is sufficiently high, the effects of the diameter-based Reynolds number $Re_D = u_j D/\nu$, where u_j, D, and ν are the jet velocity, nozzle diameter, and kinematic molecular viscosity, respectively, have been found to be strong for $Re_D \lesssim 10^5$ as pointed out in the review papers by Crighton[3] and Hussain.[4]

The influence of the Reynolds number on jet flows has been clearly described in a number of studies for jets at low Reynolds numbers, typically lower than 5×10^4, which are generally in a fully laminar initial state. Theoretical analyses conducted by Morris[5,6] and Michalke[7] based on the linear stability equations have, for instance, shown that increasing the Reynolds number raises the growth rates of instability waves. A large amount of experimental data has also been obtained for plane and round jets by Lemieux and Oosthuizen,[8] Namer and Ötügen,[9] Weisgraber

a)Electronic mail: christophe.bogey@ec-lyon.fr.

and Liepmann,[10] Papadopoulos and Pitts,[11] Kwon and Seo,[12] Deo *et al.*,[13] and Fellouah *et al.*[14] Higher Reynolds numbers generally result in a broadening of the turbulence spectra, shorter jet potential cores, lower rates of centerline velocity decay and jet spreading, and reduced peak rms levels of velocity fluctuations.

For jets at moderate Reynolds numbers, roughly between 5×10^4 and 5×10^5, the effects of the Reynolds number are still appreciable, but they are more difficult to investigate. Such jets are indeed usually in a transitional initial state, characterized by significant levels of velocity disturbances at the nozzle exit, which tend to vary with the Reynolds number as reported in a series of experiments by Zaman.[15–17] Changing the Reynolds number in this case alters the initial turbulence conditions, leading to modifications of the jet characteristics which may exceed those due to the Reynolds number alone. This issue, which was mentioned by Hussain and Zedan[18,19] and Gutmark and Ho,[20] among others, is one of the reasons why there have been intense controversies about the persistence and excitability of coherent turbulent structures in laboratory-scale mixing layers and jets at moderate Reynolds numbers. On this matter, the reader can refer to the results and discussions available in the papers by Crow and Champagne,[21] Brown and Roshko,[22] Chandrsuda *et al.*,[23] Wygnanski *et al.*,[24] Browand and Latigo,[25] Zaman and Hussain,[26,27] Crighton,[3] Hussain,[4] and Zaman.[16]

The sensitivity of jet noise to Reynolds number has also been discussed intensively over the past few decades. Similarities have been observed experimentally between acoustic measurements for jets at low, moderate, and high Reynolds numbers. This is particularly true for supersonic jets, in which instability waves and large turbulent scales play prominent roles in noise generation as explained by Tam,[28] and spectacularly illustrated by the experimental data of Morrison and McLaughlin[29] and Troutt and McLaughlin[30] for jets at Mach numbers around 2 and Reynolds numbers between 7.9×10^3 and 2.6×10^6. Despite much broader shapes for higher Re_D, the sound spectra for these jets indeed exhibit coincident peak Strouhal numbers.

For subsonic jets, some similarities remain between the sound fields of low and high Reynolds number jets as shown by the data of Stromberg *et al.*[31] for a Mach number 0.9 jet at $\mathrm{Re}_D = 3.6 \times 10^3$. It is however well known that the spectral properties of subsonic jet noise vary with the Reynolds number below a threshold value between $\mathrm{Re}_D = 10^5$ and $\mathrm{Re}_D = 4 \times 10^5$ according to authors such as Yamamoto and Arndt,[33] Long and Arndt,[34] Bridges and Hussain,[35] and Viswanathan.[36] Unfortunately, the direct effects of the Reynolds number are complicated to identify because, as indicated previously, they may be overwhelmed by the effects of other parameters dependent on Re_D. These parameters include the nozzle-exit boundary-layer thickness and disturbance levels, which have been found to have a major impact on subsonic jet noise in the experiments of Mollo-Christensen *et al.*[32] and Zaman,[15,16] as well as in the simulations of Bogey and Bailly[37] and Bogey *et al.*,[38] for instance, especially regarding the contribution of shear-layer vortex pairings.

In light of the above, it appears that there is still a need to quantify the influence of Reynolds number on subsonic jets at moderate Reynolds numbers, and that the only proper way to do so is to consider jets with effectively the same initial parameters except for Re_D. To achieve this, the use of simulations as numerical experiments under highly controlled conditions is natural given the progress made in the computation of compressible jets, see in Colonius and Lele,[39] Bailly and Bogey,[40] and Wang *et al.*,[41] for example. Direct numerical simulations or large-eddy simulations (LESs) can be performed, as was the case in past studies by Freund,[42] Bogey *et al.*,[43] Klein *et al.*,[44] Bogey and Bailly,[45,46] Kleinman and Freund,[47] and Kim and Choi.[48] The last five references[44–48] are particularly relevant here because they demonstrated the feasibility of investigating Reynolds number effects in mixing layers or jets at low or moderate Reynolds numbers by means of simulations. The flow initial state was nevertheless laminar, or weakly disturbed, in these works.

In the present work, the aim is to carefully examine the influence of moderate Reynolds numbers on the flow and sound fields of subsonic jets which are, on the contrary, initially highly disturbed. As far as we are aware, it is the first detailed study on this matter. Four isothermal round jets at a Mach number M = 0.9, and at Reynolds numbers $\mathrm{Re}_D = 2.5 \times 10^4$, 5×10^4, 10^5, and 2×10^5, respectively, are computed using LESs on a grid containing 252×10^6 points using low-dissipation numerical schemes and relaxation filtering as a subgrid dissipation model. The mesh grid and numerical methods are the same as those used in recent simulations,[38,49,50] which were shown to provide accurate solutions for jets at a constant $\mathrm{Re}_D = 10^5$. The four jets originate from a pipe

nozzle, in which a trip-like excitation is applied to the boundary layers in order to obtain peak axial turbulence intensities $u'_e/u_j \simeq 9\%$ at the exit section. A great care is also taken to maintain, at the exit, laminar mean velocity profiles of momentum thickness $\delta_\theta \simeq 0.018r_0$, where $r_0 = D/2$ is the pipe radius, in all cases. Consequently, the jets display nearly identical initial conditions except for Re_D, and the trends revealed by the simulation data will be attributed to Reynolds number effects.

The paper is organized as follows. The main parameters of the jets and of the simulations, including numerical algorithm, computational grids and times, are documented in Sec. II. In Sec. III, the nozzle-exit flow conditions are characterized. The shear-layer and jet flow fields as well as the acoustic fields are then shown and analyzed. Concluding remarks are finally provided in Sec. IV.

II. PARAMETERS

In this section, the jet inflow conditions are first defined. The numerical methods and parameters are then presented. They are identical to those used in recent jet simulations, which have been thoroughly described in previous references.[37, 38, 49, 50] Therefore, only a brief description is provided here.

The simulation of the jet at $Re_D = 10^5$ considered in the present study was moreover performed for the first time and detailed in Bogey *et al.*,[49] in which a great deal of information about the boundary-layer tripping procedure, the discretization quality and the LES reliability is available. This computation is also known as Jetring1024drdz or Jet9% in other papers.[38, 49, 50]

A. Jet definition

Four isothermal round jets, referred to as JetRe25e3, JetRe50e3, JetRe100e3, and JetRe200e3, are investigated. They are at a Mach number $M = u_j/c_a = 0.9$, where c_a is the ambient speed of sound, and at Reynolds numbers $Re_D = 2.5 \times 10^4$, 5×10^4, 10^5, and 2×10^5, respectively, as reported in Table I. For completeness, the jet velocities and diameters are also given in the table. The diameters range from $D = 0.125$ cm at $Re_D = 2.5 \times 10^4$ up to $D = 1$ cm at $Re_D = 2 \times 10^5$. The four jets originate at $z = 0$ from a pipe nozzle of radius r_0 and length $2r_0$, whose lips are $0.053r_0$ thick. The ambient temperature and pressure are $T_a = 293$ K and $p_a = 10^5$ Pa. For all jets, an axial velocity profile given by a polynomial approximation of the Blasius laminar boundary-layer profile is imposed at the pipe inlet. This profile has a thickness $\delta_0 = 0.15r_0$, yielding a momentum thickness $\delta_\theta = 0.018r_0$ similar to those measured by Zaman[15, 16] in tripped subsonic jets at Re_D between 10^5 and 2.5×10^5. Radial and azimuthal velocities are initially set to zero, pressure is set to p_a, and the temperature is determined by a Crocco-Busemann relation.

The boundary layers inside the pipe are tripped by adding random low-level vortical disturbances decorrelated in the azimuthal direction at $z = -r_0$, in order to generate highly disturbed exit conditions for the jets, whose initial state would otherwise be laminar. The excitation magnitudes are empirically chosen to obtain, at the pipe exit, peak turbulence intensities u'_e/u_j around 9% in all cases, as well as mean velocity profiles remaining similar to the laminar profiles imposed at the pipe inlet, which will be illustrated in Sec. III A. More precisely, the coefficient α specifying the forcing strength, refer to Appendix A in Bogey *et al.*,[49] is set to values of 0.133, 0.068, 0.045, and 0.03475 in JetRe25e3,

TABLE I. Jet inflow conditions: velocity u_j, diameter $D = 2r_0$, Mach and Reynolds numbers M and Re_D, inlet boundary-layer thickness δ_0 and momentum thickness δ_θ.

	u_j (m s^{-1})	D (m)	M	Re_D	δ_0/r_0	δ_θ/r_0
JetRe25e3	308	1.25×10^{-3}	0.9	2.5×10^4	0.15	0.018
JetRe50e3	308	2.5×10^{-3}	0.9	5×10^4	0.15	0.018
JetRe100e3	308	5×10^{-3}	0.9	10^5	0.15	0.018
JetRe200e3	308	10^{-2}	0.9	2×10^5	0.15	0.018

JetRe50e3, JetRe100e3, and JetRe200e3, respectively. Thus, the higher the Reynolds number, the lower the amplitude of the trip-like excitation in the boundary layers necessary to reach a given level of nozzle-exit velocity disturbances, as expected. Pressure fluctuations of maximum amplitude 200 Pa random in both space and time are also added in the shear layers between $z = 0.25r_0$ and $z = 4r_0$ from $t = 0$ up to non-dimensional time $t = 12.5r_0/u_j$ in order to speed up the initial transitory period.

B. LES procedure and numerical methods

The LESs are carried out using a solver of the three-dimensional filtered compressible Navier-Stokes equations in cylindrical coordinates (r, θ, z) based on low-dissipation and low-dispersion explicit schemes. The axis singularity is taken into account by the method of Mohseni and Colonius.[51] To alleviate the time-step restriction near the cylindrical origin, the derivatives in the azimuthal direction around the axis are calculated at coarser resolutions than permitted by the grid.[52] Fourth-order 11-point centered finite differences are used for spatial discretization, and a second-order six-stage Runge-Kutta algorithm is implemented for time integration.[53] A sixth-order 11-point centered filter[54] is applied explicitly to the flow variables every time step. Non-centered finite differences and filters are also used near the pipe walls and the grid boundaries.[37,55] The radiation conditions of Tam and Dong[56] are finally applied at all boundaries, with the addition at the outflow of a sponge zone combining grid stretching and Laplacian filtering.[57]

In the simulations, the explicit filtering is employed to remove grid-to-grid oscillations, but also as a subgrid high-order dissipation model to relax turbulent energy from scales at wave numbers close to the grid cut-off wave number while leaving larger scales mostly unaffected.[45,58,59] With this in mind, the reliability of the LES fields in JetRe100e3 has been studied in Bogey *et al.*[49] based on the transfer functions associated with molecular viscosity, explicit (relaxation) filtering, and time integration. Viscosity was shown to be the dominant dissipation mechanism for scales discretized at least by seven points per wavelength. The physics of the larger structures are therefore expected not to be governed by numerical or subgrid-modeling dissipation in JetRe100e3, which implies in particular that the effective flow Reynolds number should not be artificially decreased. This remark certainly equally holds for the simulations JetRe25e3 and JetRe50e3 dealing with jets at lower Reynolds numbers using the same grid. This is also likely the case for JetRe200e3 in which the jet Reynolds number is only slightly higher than that in JetRe100e3.

C. Simulation parameters

As indicated in Table II, the LESs are performed using a grid containing $n_r \times n_\theta \times n_z = 256 \times 1024 \times 962 = 252 \times 10^6$ points. There are 169 points along the pipe nozzle, 77 points within the jet radius, and 31 points inside the inlet boundary layers. The physical domain, excluding the 80-point outflow sponge zone, extends axially up to $L_z = 25r_0$, and radially up to $L_r = 9r_0$.

The mesh spacing is uniform in the azimuthal direction, with $r_0\Delta\theta = 0.0061r_0$. In the axial direction, the mesh spacing is minimum between $z = -r_0$ and $z = 0$, with $\Delta z = 0.0072r_0$. It increases upstream of $z = -r_0$, but also downstream of the nozzle at stretching rates lower than 1% allowing to reach $\Delta z = 0.065r_0$ between $z = 13.3r_0$ and $z = L_z = 25r_0$. In the radial direction, the mesh spacing is minimum around $r = r_0$, with $\Delta r = 0.0036r_0$. It is equal to $\Delta r = 0.292r_0$ close to the jet axis, to $\Delta r = 0.081r_0$ between $r = 3r_0$ and $r = 6.75r_0$, and finally to $\Delta r = 0.176r_0$ at $r = L_r = 9r_0$. Further details regarding the mesh spacings, as well as representations of the variations of Δz and Δr with z and r, respectively, can be found in previous papers.[38,49]

TABLE II. Simulation parameters: numbers of grid points n_r, n_θ, n_z, mesh spacings Δr at $r = r_0$, $r_0\Delta\theta$, and Δz at $z = 0$, extents L_r, L_z of the physical domain, radial position r_c of the far-field extrapolation surface, and time duration T.

n_r, n_θ, n_z	$\Delta r/r_0$	$r_0\Delta\theta/r_0$	$\Delta z/r_0$	L_r, L_z	r_c/r_0	Tu_j/r_0
256, 1024, 962	0.36%	0.61%	0.72%	$9r_0, 25r_0$	6.5	375

The quality of the discretization in JetRe100e3 has been assessed in Bogey *et al.*[49] The ratios between the integral length scales of the axial fluctuating velocity and the mesh spacings along the lip line were shown to fall between 4 and 10. The properties of the nozzle-exit turbulence and of the shear-layer flow fields were moreover found to be practically insensitive to a further refinement of the grid. The grid resolution is thus expected to be appropriate in JetRe100e3, as well as in JetRe25e3 and JetRe50e3 for the lower Reynolds number jets in which the contribution of fine-scale turbulence is naturally weakened. The resolution is also probably sufficient for the jet at $Re_D = 2 \times 10^5$, in which, according to a number of observations in free shear flows,[4,20,22,24,27,44,47] the increase of the Reynolds number by a factor of two with respect to JetRe100e3 should produce more small-scale structures without fundamentally altering the large-scale.

The simulation time, given in Table II, is equal to $375r_0/u_j$ in all cases. After the initial transitory period, density, velocity components, and pressure are recorded from time $t = 100r_0/u_j$ along the jet axis, and on two surfaces at $r = r_0$ and $r = r_c = 6.5r_0$, at a sampling frequency allowing the computation of spectra up to a Strouhal number of $St_D = fD/u_j = 20$, where f is the time frequency. The cylindrical surface surrounding the jets is located at $r = 6.5r_0$ because, as indicated previously, the radial mesh spacing is uniform for $3r_0 \leq r \leq 6.75r_0$ but then increases for $r \geq 6.75r_0$. The radial mesh spacing at $r = 6.5r_0$ furthermore yields a Strouhal number of $St_D = fD/u_j = 6.9$ for an acoustic wave discretized by four points per wavelength. In the azimuthal direction, for practical reasons, every fourth grid point is stored, implying that data post-processing is possible up to an azimuthal mode $n_\theta = 128$, where n_θ is the dimensionless azimuthal wave number such that $n_\theta = k_\theta r$. The velocity spectra are evaluated from overlapping samples of duration $27.4r_0/u_j$. The flow statistics are determined from $t = 175r_0/u_j$, and they are averaged in the azimuthal direction. They can be considered to be well converged in view of the results of recent studies[38,49] and of those obtained at intermediary stages of the present LESs for $t \geq 300r_0/u_j$. In JetRe50e3, for example, the mean and rms velocity profiles calculated at $t = 320r_0/u_j$ and at $t = 375r_0/u_j$ are found to be in good agreement. The differences do not exceed 1% for the peak turbulence intensity values.

The simulations have been performed using NEC SX-8 computers, on 7 processors using OpenMP, leading to a central processing unit (CPU) speed of around 36 Gflops. Each LES required around 7000 CPU h and 60 Gb of memory for 164 000 time steps.

D. Far-field extrapolation

The LES near fields are propagated to the acoustic far field by solving the isentropic linearized Euler equations (ILEE) in cylindrical coordinates.[37,38,49,60] The extrapolation is performed from fluctuating velocities and pressure recorded in the LESs on a surface at $r = 6.5r_0$ as mentioned above. Concerning the position of the surface, it can be noted that very similar far-field results were obtained using two surfaces at $r = 5.25r_0$ and at $r = 7.25r_0$ in Bogey and Bailly[37] for an initially laminar jet. The data at $r = 6.5r_0$ are interpolated onto a cylindrical surface discretized by an axial mesh spacing of $\Delta z = 0.065r_0$. They are then imposed at the bottom boundary of the grid on which the ILEE are solved using the same numerical methods as in the LESs. This grid contains 845 $\times$ 256 $\times$ 1155 points, and extends axially from $z = -16.6r_0$ to $58.2r_0$ and radially up to $r = 61.4r_0$. The grid spacings are uniform with $\Delta r = \Delta z = 0.065r_0$, yielding $St_D = 8.6$ for an acoustic wave at four points per wavelength. After a propagation time of $t = 60r_0/u_j$, pressure is recorded around the jets at a distance of $60r_0$ from $z = r = 0$, where far-field acoustic conditions are expected to apply according to the experiments of Ahuja *et al.*,[61] during a period of $250r_0/u_j$. Pressure spectra are evaluated using overlapping samples of duration $38r_0/u_j$, and they are averaged in the azimuthal direction.

III. RESULTS

A. Nozzle-exit flow conditions

The profiles of mean and rms axial velocities obtained at the nozzle exit of the jets are presented in Figure 1. They appear not to vary much with the Reynolds number, as was intended. In

TABLE III. Nozzle-exit conditions: peak turbulence intensity u'_e/u_j, shape factor H and momentum thickness $\delta_\theta(0)$ of the boundary layers, and Reynolds number Re_θ based on $\delta_\theta(0)$; and flow properties calculated from velocity u'_z at $r = r_0$ and $z = 0.4r_0$: axial and azimuthal integral length scales $L_{uu}^{(z)}$ and $L_{uu}^{(\theta)}$, ratio $L_{uu}^{(z)}/L_{uu}^{(\theta)}$, and sums of coefficients $a_{uu}^{(\theta)}$ obtained from the correlation functions $\mathcal{R}_{uu}^{(\theta)}$, refer to expressions (1).

	u'_e/u_j	H	$\delta_\theta(0)/r_0$	Re_θ	$L_{uu}^{(z)}/r_0$	$L_{uu}^{(\theta)}/r_0$	$L_{uu}^{(z)}/L_{uu}^{(\theta)}$	$a_{uu}^{(\theta)}\vert_{VLS}$	$a_{uu}^{(\theta)}\vert_{LS}$	$a_{uu}^{(\theta)}\vert_{FS}$
JetRe25e3	9.12%	2.18	0.0201	256	0.102	0.021	4.79	0.252	0.697	0.051
JetRe50e3	9.20%	2.30	0.0191	486	0.076	0.016	4.85	0.202	0.657	0.141
JetRe100e3	9.18%	2.36	0.0185	943	0.058	0.013	4.33	0.163	0.612	0.225
JetRe200e3	9.13%	2.40	0.0183	1856	0.048	0.012	4.16	0.149	0.587	0.264

Figure 1(a), the mean velocity profiles are all similar to the Blasius laminar profile specified at the pipe-nozzle inlet. Small shape modifications, indicative of early stages of transition towards turbulent mean velocity profiles, are however observed as the Reynolds number decreases, leading to a shape factor ranging from $H = 2.40$ at $\mathrm{Re}_D = 2 \times 10^5$ down to $H = 2.18$ at $\mathrm{Re}_D = 2.5 \times 10^4$, refer to Table III for all flow parameters at $z = 0$. The exit boundary-layer momentum thickness $\delta_\theta(0)$ also changes a little with Re_D. It is equal to 2.01%, 1.91%, 1.85%, and 1.83% of the nozzle radius in JetRe25e3, JetRe50e3, JetRe100e3, and JetRe200e3, respectively, yielding Reynolds numbers $\mathrm{Re}_\theta = u_j\delta_\theta(0)/\nu = 256$, 486, 943, and 1856. Viscosity effects should consequently be strong in the shear layers of the jets at lower Re_D, but much weaker at higher Re_D. In Figure 1(b), the rms velocity profiles show significant values over a slightly wider zone for lower Re_D, as a result of the variations of $\delta_\theta(0)$, but the peak turbulence intensity remains very close to 9% in all cases. The shear layers of the present jets are therefore characterized by nearly the same initial conditions except for the Reynolds number Re_θ. These conditions correspond to those found in highly disturbed, or nominally (not fully) turbulent, boundary layers.[15, 16, 18, 19, 50] In particular, they are shown to be comparable to those measured by Zaman[15, 16] about $0.1r_0$ downstream of the exit section of a tripped jet at $\mathrm{Re}_D = 10^5$.

As usually done to evaluate the size of large scales in turbulent flows, integral length scales are computed from fluctuating velocity u'_z at $r = r_0$ and $z = 0.4r_0$ on the nozzle lip line. This location is arbitrarily chosen very close to the nozzle exit in order to avoid the turbulence properties being appreciably affected by the mixing-layer development. The length scales $L_{uu}^{(z)}$ and $L_{uu}^{(\theta)}$ obtained in the axial and azimuthal directions are given in Table III, and presented in Figure 2(a) as functions of Re_D and Re_θ. They both decrease monotonically with increasing Reynolds numbers, from $L_{uu}^{(z)} = 0.102r_0$ and $L_{uu}^{(\theta)} = 0.021r_0$ in JetRe25e3 down to $L_{uu}^{(z)} = 0.048r_0$ and $L_{uu}^{(\theta)} = 0.012r_0$ in JetRe200e3. This is most probably due to the generation of more fine-scale structures, refer to the velocity spectra of Figure 3 below. The ratio $L_{uu}^{(z)}/L_{uu}^{(\theta)}$ between the integral length scales is however noted in Table III and in Figure 2(b) not to vary appreciably, and to have values around 4.5 regardless of Re_D.
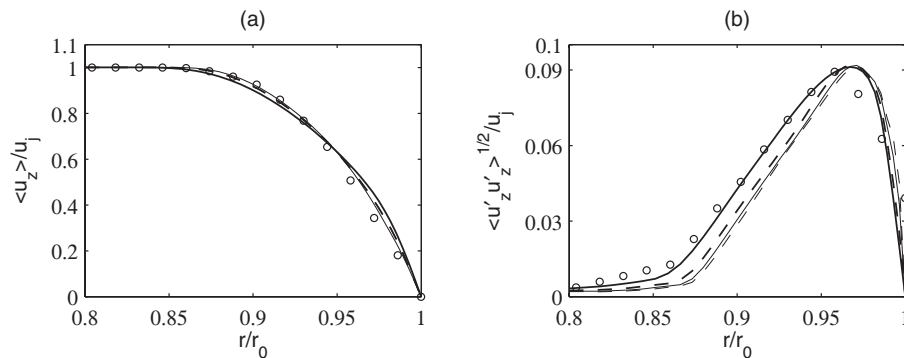

FIG. 1. Profiles at $z = 0$ (a) of mean axial velocity $\langle u_z \rangle$ and (b) of the rms values of fluctuating axial velocity u'_z: (bold solid) JetRe25e3, (bold dashed) JetRe50e3, (thin solid) JetRe100e3, (thin dashed) JetRe200e3, (circle) measurements of Zaman[15, 16] for a Mach 0.18, tripped jet at $\mathrm{Re}_D = 10^5$ about $0.1r_0$ downstream of the exit plane.
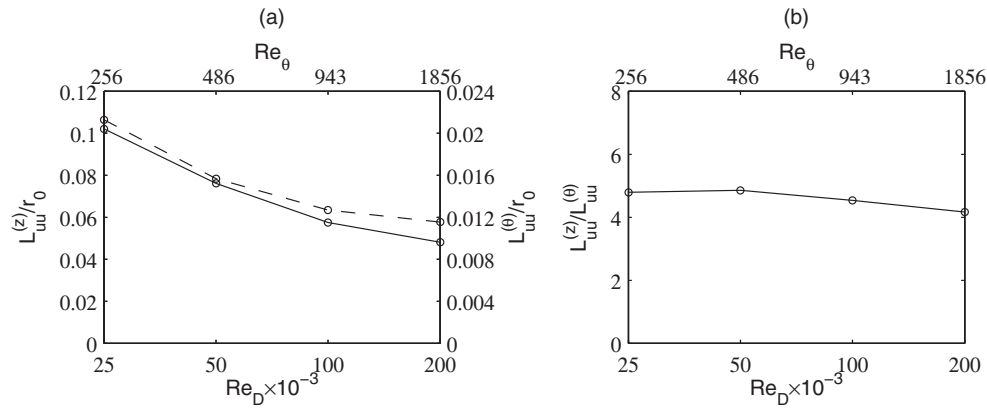
FIG. 2. Variations with the Reynolds numbers Re_D and Re_θ (a) of the axial and azimuthal integral length scales (bold solid) $L_{uu}^{(z)}$ and (bold dashed) $L_{uu}^{(\theta)}$, and (b) of the ratio $L_{uu}^{(z)}/L_{uu}^{(\theta)}$, calculated from velocity u_z' at $r = r_0$ and $z = 0.4r_0$.

This result suggests that the turbulent structures initially dominating in the jet mixing layers are of similar nature despite the difference in Reynolds number. Based on $L_{uu}^{(z)}/L_{uu}^{(\theta)}$, they are elongated in the axial direction, as expected for structures developing in turbulent boundary layers, which will be discussed in what follows.

As in our previous studies on tripped jets,[38,49,50] the properties of the jet initial disturbances are examined by calculating spectra of the fluctuating axial velocity at $r = r_0$ and $z = 0.4r_0$, at the same position as the integral length scales. The spectra are represented as a function of the Strouhal number $St_D = fD/u_j$ in Figure 3(a), and of the azimuthal mode n_θ in Figure 3(b). With increasing Reynolds number, the spectra are seen to broaden. More precisely, the contributions of higher frequency components, noticed here for Strouhal numbers $St_D \gtrsim 3$ and azimuthal modes $n_\theta \gtrsim 60$, become stronger, whereas those of lower frequency components are slightly reduced. The shapes of the spectra however do not change fundamentally. For all jets, indeed, the frequency spectra in Figure 3(a) are rather flat up to $St_D \simeq 1$ and decrease for higher Strouhal numbers. In the same way, the spectra in Figure 3(b) all show a distribution of turbulent energy over a very large number of azimuthal modes with peak components centered around $k_\theta \simeq 42$, or $k_\theta \delta_0/r_0 \simeq 7$ when normalized by the boundary-layer thickness. Similar spectral features were obtained by Eggels *et al.*[62] for a fully turbulent pipe flow at $Re_\theta = 236$, and by Tomkins and Adrian[63] for turbulent boundary layers at $Re_\theta = 1015$ and 7705, that is, for Reynolds numbers lying roughly within the range $Re_\theta = 256 - 1856$ considered in this work. This was pointed out in a recent note[50] on that specific subject, which also provided comparisons with data of the literature. Therefore, even if differences exist between pipes/channels and boundary layers,[62,64–66] similarities are noted between the large-scale
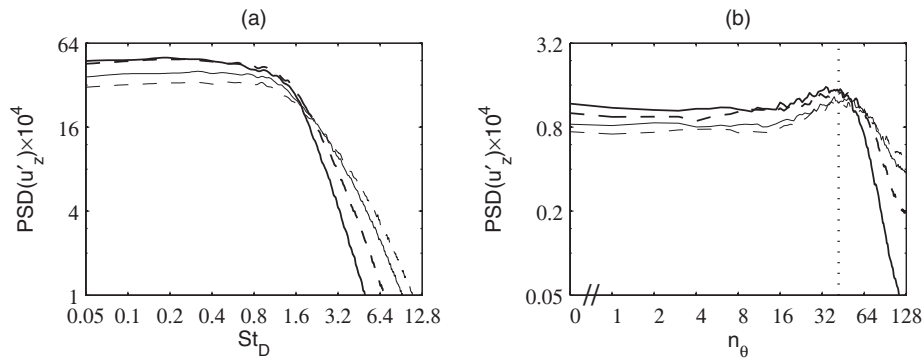

FIG. 3. Power spectral densities (PSD) normalized by u_j of fluctuating velocity u_z' at $r = r_0$ and $z = 0.4r_0$, as functions (a) of Strouhal number $St_D = fD/u_j$ and (b) of azimuthal mode n_θ: (bold solid) JetRe25e3, (bold dashed) JetRe50e3, (thin solid) JetRe100e3, (thin dashed) JetRe200e3. The dotted line indicates $n_\theta = 42$.
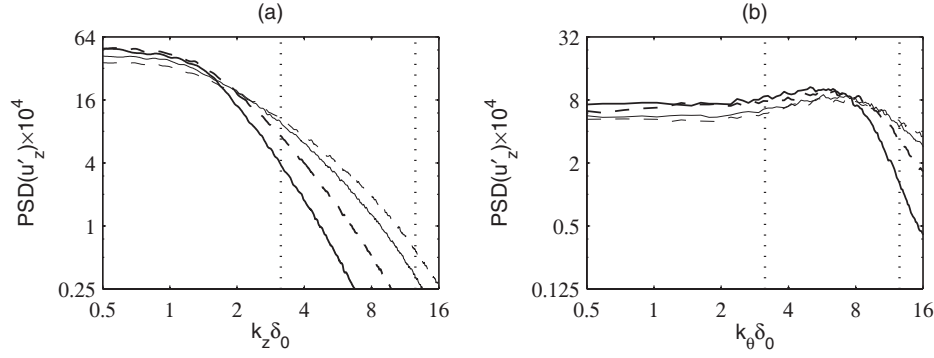
FIG. 4. Power spectral densities normalized by u_j of velocity u'_z at $r = r_0$ and $z = 0.4r_0$, as functions of non-dimensional axial and azimuthal wave numbers (a) $k_z\delta_0$ and (b) $k_\theta\delta_0$: (bold solid) JetRe25e3, (bold dashed) JetRe50e3, (thin solid) JetRe100e3, (thin dashed) JetRe200e3. The dotted lines indicate $k_z\delta_0 = k_\theta\delta_0 = \pi$ and 4π, yielding $\lambda_z = \lambda_\theta = 2\delta_0$ and $\delta_0/2$, respectively.

structures at the pipe-nozzle exit of the present tripped jets and those in turbulent wall-bounded flows. These structures appear to depend weakly on the Reynolds number.

It is interesting to compare the integral length scales with the length scales corresponding to the components dominating in the velocity spectra, which both can be considered as characteristic sizes of the eddies containing most of the turbulent energy. At $r = r_0$ and $z = 0.4r_0$, they are found to differ qualitatively as well as quantitatively. The integral length scales indeed vary significantly with the Reynolds number, whereas the dominant length scales do not. The former are furthermore much smaller than the latter, undoubtedly because they are based on all turbulent structures, including the finer ones. In the azimuthal direction, there is in particular about an order of magnitude discrepancy between $L_{uu}^{(\theta)} = 0.012r_0 - 0.021r_0$ and the structure spacings $\lambda_\theta \simeq 0.15r_0$ associated with the peak azimuthal modes, the above value being equal to the boundary-layer thickness δ_0.

To more clearly identify the most influential scales of turbulence, the velocity spectra of Figure 3 are re-plotted in Figure 4 versus axial and azimuthal wave numbers $k_z\delta_0$ and $k_\theta\delta_0$, using a scaling[38,50] with δ_0. Wavelengths $\lambda_z = \lambda_\theta = 2\delta_0$ and $\delta_0/2$ are also indicated by dotted lines at $k_z\delta_0 = k_\theta\delta_0 = \pi$ and 4π, respectively. The distribution of turbulent energy is found to be fundamentally different in the axial and azimuthal directions. Dominant spectral components correspond to very large scales with $k_z\delta_0 \leq 1.2$ and wavelengths λ_z typically greater than $5\delta_0$ in the former case, but to scales in the range of wavelengths $\delta_0/2 \leq \lambda_\theta \leq 2\delta_0$ in the latter.

To quantify the trends exhibited in Figure 4(b), three truncated sums of Fourier coefficients $a_{uu}^{(\theta)}$ obtained from the decomposition of cross-correlation functions $\mathcal{R}_{uu}^{(\theta)}$ of velocity u'_z with the azimuthal modes at $r = r_0$ and $z = 0.4r_0$ are considered. They are defined as

$$\begin{cases} a_{uu}^{(\theta)}|_{VLS} = \sum a_{uu}^{(\theta)}|_{\lambda_\theta \geq 2\delta_0} \\ a_{uu}^{(\theta)}|_{LS} = \sum a_{uu}^{(\theta)}|_{\delta_0/2 \leq \lambda_\theta \leq 2\delta_0} \\ a_{uu}^{(\theta)}|_{FS} = \sum a_{uu}^{(\theta)}|_{\lambda_\theta \leq \delta_0/2 \ \& \ n_\theta \leq 128} \end{cases} \tag{1}$$

so as to estimate percentages of energy in the very large, large, and fine-scale structures in the azimuthal direction. In practice, they are, respectively, performed for $0 \leq n_\theta \leq 20$, $21 \leq n_\theta \leq 80$, and $81 \leq n_\theta \leq 128$ since $n_\theta = 128$ is the highest mode available from the LES data base. The sum $a_{uu}^{(\theta)}|_{FS}$ therefore does not represent but is lower than the truncated sum which would be calculated up to the grid cut-off azimuthal mode $n_\theta = 512$. Given the amplitude of higher components in Figure 3(b), the difference is expected to be negligible for $\mathrm{Re}_D = 2.5 \times 10^4$, and more notable with increasing Reynolds number. The values of $a_{uu}^{(\theta)}|_{VLS}$, $a_{uu}^{(\theta)}|_{LS}$ and $a_{uu}^{(\theta)}|_{FS}$ are provided in Table III, and displayed in Figure 5 as functions of the Reynolds numbers. The contribution of the structures with $\delta_0/2 \leq \lambda_\theta \leq 2\delta_0$ predominates in all cases. It however decreases slightly with Re_D, from 69.7% in JetRe25e3 down to 58.7% in JetRe200e3. A similar reduction, from 25.2% to 14.9%, is observed for the contribution of the wavelengths greater than twice the boundary-layer thickness. On the
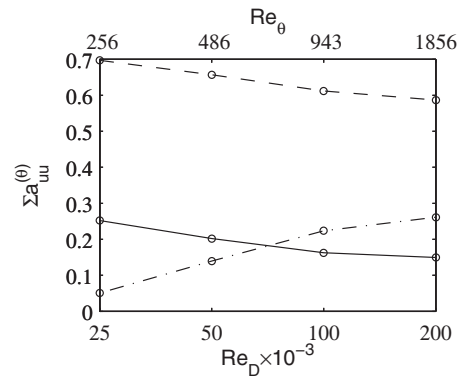
FIG. 5. Variations with Re_D and Re_θ of the truncated sums of coefficients $a_{uu}^{(\theta)}$ obtained from functions $\mathcal{R}_{uu}^{(\theta)}$ at $r = r_0$ and $z = 0.4r_0$: (solid) $a_{uu}^{(\theta)}|_{VLS}$, (dashed) $a_{uu}^{(\theta)}|_{LS}$, (dotted-dashed) $a_{uu}^{(\theta)}|_{FS}$.

contrary, the percentage of energy in the finer scales with $\lambda_\theta \leq \delta_0/2$ increases strongly, from a small value of 5.1% at $Re_D = 2.5 \times 10^4$ to a significant value of 26.4% at $Re_D = 2 \times 10^5$.

B. Shear-layer development

Vorticity fields obtained from the pipe-nozzle exit up to $z = 5r_0$ in the jet shear layers are represented in Figure 6 and in movie 1. For the jet at $Re_D = 2.5 \times 10^4$, large-scale structures are clearly visible in Figure 6(a), which is not surprising given the momentum-thickness-based Reynolds number $Re_\theta = 256$ in this case. The shear layer shows structures elongated in the streamwise direction near the pipe exit, corresponding to those observed in turbulent boundary layers[63,67] as argued above and in a previous paper.[50] It seems to roll up around $z = 1.5r_0$, and then to exhibit, farther downstream, large-scale structures resembling the coherent vortical structures revealed by the well-known visualizations of Brown and Roshko.[22] With increasing Reynolds number, there is a gradual appearance of fine-scale turbulence, and large-scale structures are more difficult to distinguish, see in particular Figure 6(d) for the jet at $Re_D = 2 \times 10^5$ (and $Re_\theta = 1856$). The vorticity fields finally suggest that the shear layers develop more slowly at higher Reynolds numbers.

To illustrate the organization of the shear-layer turbulent structures in the azimuthal direction, snapshots of the axial vorticity ω_z obtained in three sections at $z = r_0$, $z = 2r_0$, and $z = 4r_0$, from top to bottom, are presented in Figure 7. At the first position at $z = r_0$, the vorticity field changes
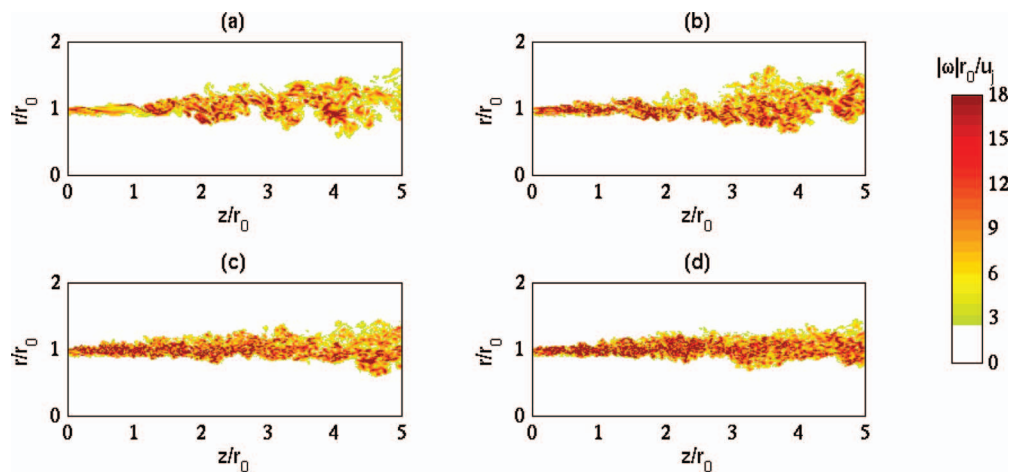

FIG. 6. Snapshots in the (z, r) plane of vorticity norm $|\boldsymbol{\omega}|$ in the shear layer downstream of the pipe lip up to $z = 5r_0$: (a) JetRe25e3, (b) JetRe50e3, (c) JetRe100e3, (d) JetRe200e3. Only $r \geq 0$ is shown (enhanced online) [URL: http://dx.doi.org/10.1063/1.4757667.1].
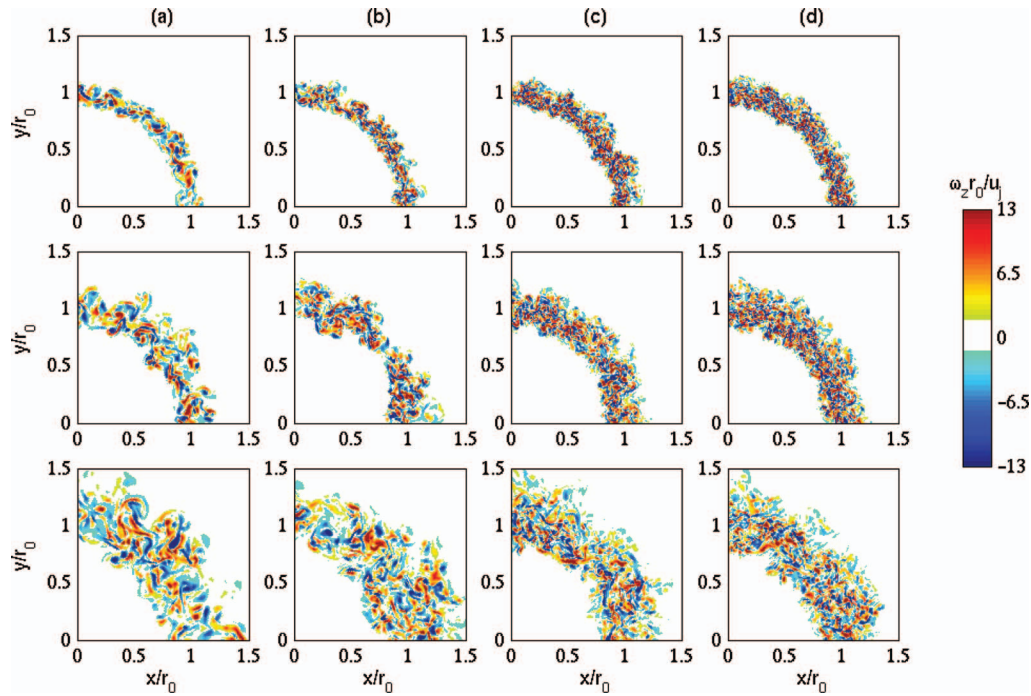
FIG. 7. Snapshots in the (r, θ) or (x, y) planes at $z = r_0$, $2r_0$ and $4r_0$, from top to bottom, of axial vorticity ω_z: (a) JetRe25e3, (b) JetRe50e3, (c) JetRe100e3, (d) JetRe200e3. Only $x, y \geq 0$ is shown.

appreciably as Re_D, and consequently Re_θ, vary. As was previously the case in the (x, y) plane, large-scale structures appear clearly in JetRe25e3, whereas fine-scale turbulence tends to dominate in the jets at higher Reynolds numbers. These trends persist, albeit attenuated, farther downstream at $z = 2r_0$ and $z = 4r_0$. It can also be emphasized that turbulence in the present initially highly disturbed jets is noticed to be fully three-dimensional in all three sections. There is notably no evidence of the presence of the axisymmetric or Kelvin-Helmholtz structures typically found in initially laminar jets,[37, 38] even in the jet at $Re_D = 2.5 \times 10^4$ displaying coherent-like vortical structures in Figure 6(a).

The axial and azimuthal integral length scales $L_{uu}^{(z)}$ and $L_{uu}^{(\theta)}$ evaluated from velocity u_z' at $r = r_0$ along the lip line are presented in Figure 8. After a short period of decrease just downstream of the nozzle exit, they are both observed to grow fairly linearly, which is in good agreement with the experimental data available in the literature for mixing layers and jets.[23, 68–71] They are also
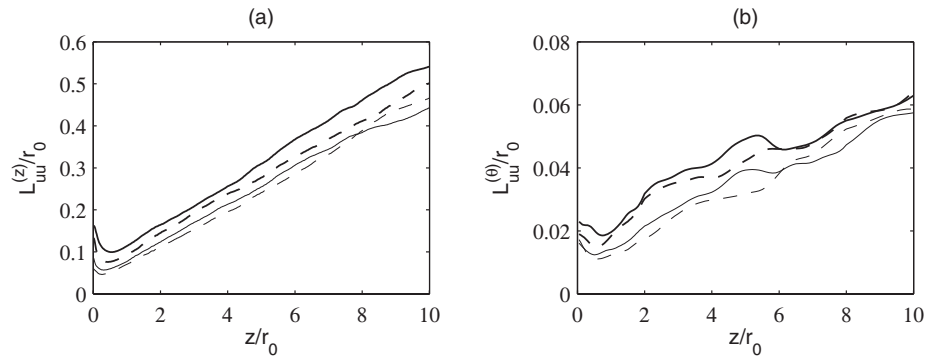

FIG. 8. Variations of axial and azimuthal integral length scales (a) $L_{uu}^{(z)}$ and (b) $L_{uu}^{(\theta)}$ calculated from velocity u_z' at $r = r_0$: (bold solid) JetRe25e3, (bold dashed) JetRe50e3, (thin solid) JetRe100e3, (thin dashed) JetRe200e3.
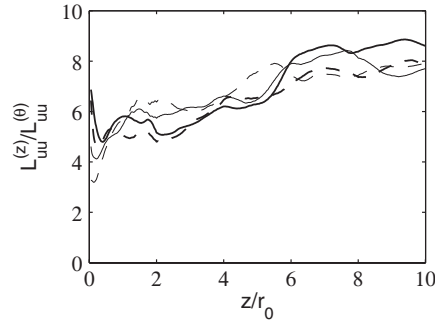
FIG. 9. Variations of the ratio $L_{uu}^{(z)}/L_{uu}^{(\theta)}$ between integral length scales at $r = r_0$: (bold solid) JetRe25e3, (bold dashed) JetRe50e3, (thin solid) JetRe100e3, (thin dashed) JetRe200e3.

seen to decrease gradually with the Reynolds number throughout the mixing layers, in comparable proportions in the two directions considered.

To give further insight into the integral characteristics of the shear-layer turbulence, the ratios $L_{uu}^{(z)}/L_{uu}^{(\theta)}$ computed between the integral length scales at $r = r_0$ are presented in Figure 9. The curves thus drawn do not appear to depend much on the Reynolds number. Overall, the ratio $L_{uu}^{(z)}/L_{uu}^{(\theta)}$ increases with the axial distance, from values around 4.5 close to the pipe exit as shown in Figure 2(b), to values around 8 farther downstream at $z \simeq 8r_0 - 10r_0$. The latter value compares well with the experimental data obtained by Morris and Zaman[72] at $r = r_0$ and $z = 10r_0$ in a jet at $\mathrm{Re}_D = 3 \times 10^5$.

The variations over $0 \leq z \leq 10r_0$ of the shear-layer momentum thickness δ_θ are presented in Figure 10(a). In accordance with the vorticity fields of Figure 6, they show that the mixing layers develop more slowly with increasing Reynolds number. To quantify this tendency, the shear-layer spreading rates $d\delta_\theta/dz$ are depicted in Figure 10(b). Their profiles vary significantly with Re_D, in terms of both amplitude and shape. For the jet at $\mathrm{Re}_D = 2.5 \times 10^4$ (and $\mathrm{Re}_\theta = 256$), the spreading rate rapidly rises downstream of the pipe exit to reach values of around 0.03 at $z \simeq 1.5r_0$, that is the position where a rolling-up of the shear layer is guessed in Figure 6(a). It remains close to this value up to $z \simeq 4r_0$, and then decreases gently down to about 0.24 at $z = 10r_0$. At higher Reynolds numbers, the spreading rates are lower, especially during the early stage of mixing-layer growth. For the jet at $\mathrm{Re}_D = 2 \times 10^5$ (and $\mathrm{Re}_\theta = 1856$), in particular, they do not exceed 0.02 upstream of $z = 3.3r_0$. A small hump is nevertheless observed in the vicinity of the pipe exit, which is in agreement with measurements provided by Husain and Hussain[73] for initially turbulent axisymmetric mixing layers at $\mathrm{Re}_\theta \simeq 1400$. Downstream of $z \simeq 8r_0$, the spreading rates from the four jet LESs appear moreover relatively similar. This behaviour can be related to experimental results of Hussain and
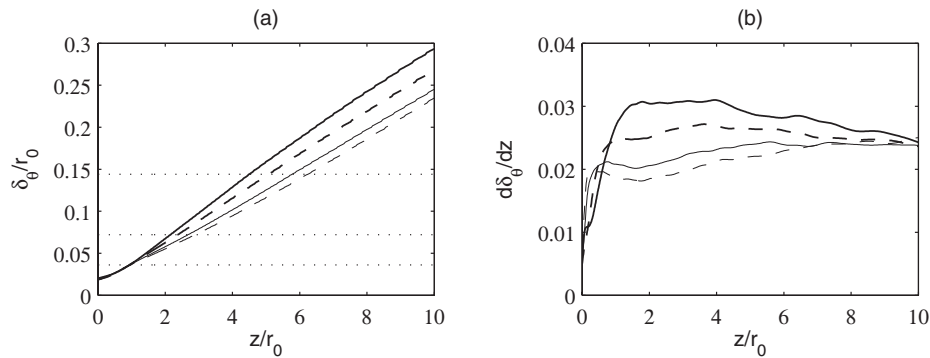

FIG. 10. Variations (a) of shear-layer momentum thickness δ_θ and (b) of spreading rate $d\delta_\theta/dz$: (bold solid) JetRe25e3, (bold dashed) JetRe50e3, (thin solid) JetRe100e3, (thin dashed) JetRe200e3. The dotted lines indicate $\delta_\theta = 0.036r_0$, $0.072r_0$, and $0.144r_0$.
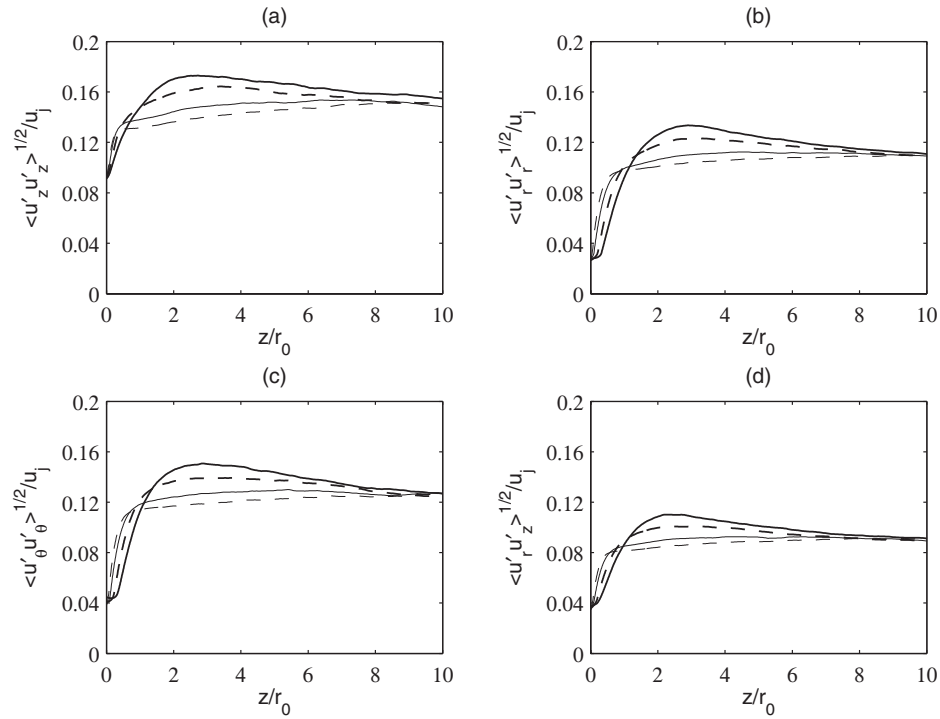
FIG. 11. Variations of the peak rms values of fluctuating velocities (a) u'_z, (b) u'_r, (c) u'_θ, and (d) of the peak magnitudes of Reynolds shear stress $\langle u'_r u'_z \rangle$: (bold solid) JetRe25e3, (bold dashed) JetRe50e3, (thin solid) JetRe100e3, (thin dashed) JetRe200e3.

Zedan,[18] who obtained asymptotic spreading rates nearly independent of the Reynolds number in mixing layers at $Re_\theta = 184 - 349$, all characterized initially by laminar mean velocity profiles and turbulence intensities $u'_e/u_j \simeq 6\%$.

The peak rms values of axial, radial, and azimuthal velocities u'_z, u'_r, and u'_θ and the maximum Reynolds shear stresses $\langle u'_r u'_z \rangle$ are represented in Figure 11 between $z = 0$ and $z = 10 r_0$. The profiles obtained for the jet at $Re_D = 2.5 \times 10^4$ all exhibit a well-marked overshoot about two radii downstream of the nozzle exit. Peak rms values $\langle u'^2_z \rangle^{1/2} = 0.173 u_j$ and $\langle u'^2_r \rangle^{1/2} = 0.133 u_j$ are reached, for example. Farther downstream, the profiles slowly decrease, and values such as $\langle u'^2_z \rangle^{1/2} \simeq 0.15 u_j$ and $\langle u'^2_r \rangle^{1/2} \simeq 0.11 u_j$ are observed at $z = 10 r_0$. For higher Reynolds numbers, after a sharper initial growth, the turbulence intensity profiles become smoother. The humps located around $z = 2 r_0$ are reduced, and even disappear at $Re_D = 2 \times 10^5$, yielding monotonically increasing profiles in that case. As the Reynolds number rises, the shear layers consequently develop with lower turbulence intensities, leading, for instance, to peak rms values of u'_z and u'_r of only $0.151 u_j$ and $0.111 u_j$ in JetRe200e3, refer also to Table IV. At larger distances from the nozzle, the fluctuation levels seem however to tend towards similar values regardless of the Reynolds number. Comparable results can be found in the paper of Hussain and Zedan.[18] For initially laminar mixing layers with constant $u'_e/u_j \simeq 6\%$ and Re_θ varying between 184 and 349, these authors indeed measured axial

TABLE IV. Peak values of turbulence intensities in the jets.

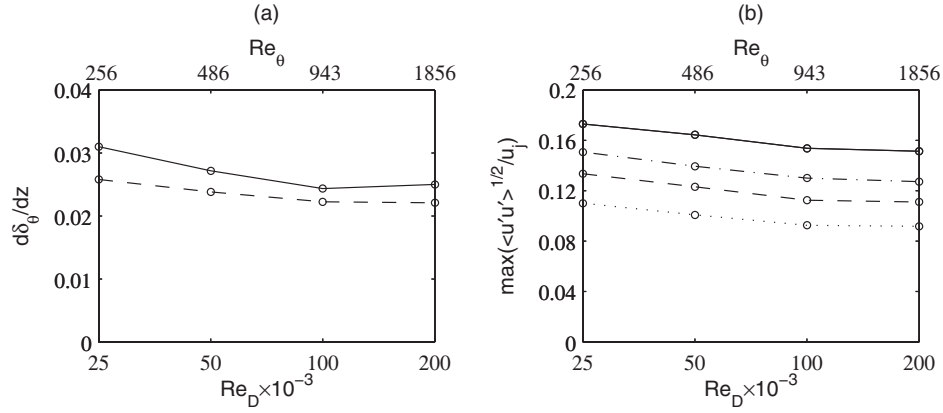|	$\langle u'^2_z \rangle^{1/2}/u_j$	$\langle u'^2_r \rangle^{1/2}/u_j$	$\langle u'^2_\theta \rangle^{1/2}/u_j$	$\langle u'_r u'_z \rangle/u_j$
JetRe25e3	17.3%	13.3%	15.1%	11.0%
JetRe50e3	16.4%	12.3%	13.9%	10.1%
JetRe100e3	15.4%	11.2%	13.0%	9.3%
JetRe200e3	15.1%	11.1%	12.7%	9.2%

FIG. 12. Variations with Re_D and Re_θ (a) of the shear-layer spreading rates $d\delta_\theta/dz$: (solid) peak values and (dashed) mean values between $z = 0$ and z_c; and (b) of the peak values of turbulence intensities: (solid) $\langle u_z'^2 \rangle^{1/2}/u_j$, (dashed) $\langle u_r'^2 \rangle^{1/2}/u_j$, (dotted-dashed) $\langle u_\theta'^2 \rangle^{1/2}/u_j$, (dotted) $\langle u_r' u_z' \rangle^{1/2}/u_j$.

turbulence intensity profiles showing a hump shortly downstream of the nozzle, and then relaxing to nearly identical values. It further appeared that the peak values are around 19% at $Re_\theta = 184$ but 17% at $Re_\theta = 349$, which is in line with the present LES data.

The present results, summarized in Figure 12 displaying the variations of the shear-layer spreading rates and peak turbulence intensities with Re_D and Re_θ, show that the mean and turbulent developments of the mixing layers become smoother with higher Reynolds numbers. Similar albeit stronger effects were obtained in recent simulations[38] of jets at $Re_D = 10^5$ when increasing the nozzle-exit disturbance levels u_e' from about 0%–12% of the jet velocity u_j. Based on an in-depth analysis of the shear-layer turbulent fields, these effects were attributed to the weakening of large-scale vortices and of their interactions, including the first stage of pairings, downstream of the nozzle exit. The aim is now to investigate whether such modifications of the flow structural characteristics arise when the jet Reynolds number varies.

Spectra of the radial velocity u_r' are computed at $z = r_0$ on the lip line, and plotted in Figure 13(a) as a function of the Strouhal number St_D. With increasing Reynolds number, they become broader, as expected. They remain however dominated by low-frequency components centered around $St_D = 1.4$, yielding $St_\theta \simeq f\delta_\theta(0)/u_j = 0.013$. This value corresponds well to the frequencies which were found to predominate early on in initially laminar annular mixing layers in theoretical analyses[5–7] and experiments,[20,74] see also the linear stability analysis conducted in Bogey *et al.*[38] for a base-flow profile representative of those in the simulated jets. Moreover, for Re_θ higher than 200 and for Re_D between 10^4 and 10^5, according to Morris,[5] Gutmark and Ho[20] and Drubka *et al.*,[74] these frequencies
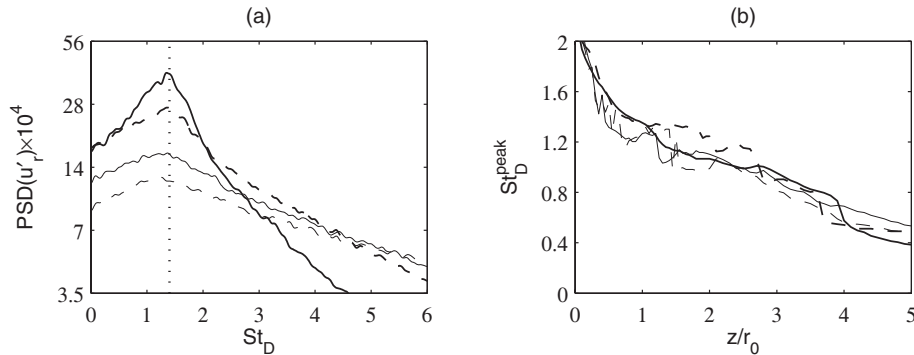

FIG. 13. Spectral properties of radial velocity u_r' at $r = r_0$; (a) power spectral densities at $z = r_0$, normalized by u_j, as functions of St_D, (b) variations of the peak Strouhal number St_D^{peak} in the PSD: (bold solid) JetRe25e3, (bold dashed) JetRe50e3, (thin solid) JetRe100e3, (thin dashed) JetRe200e3. The dotted line indicates $St_D = 1.4$.
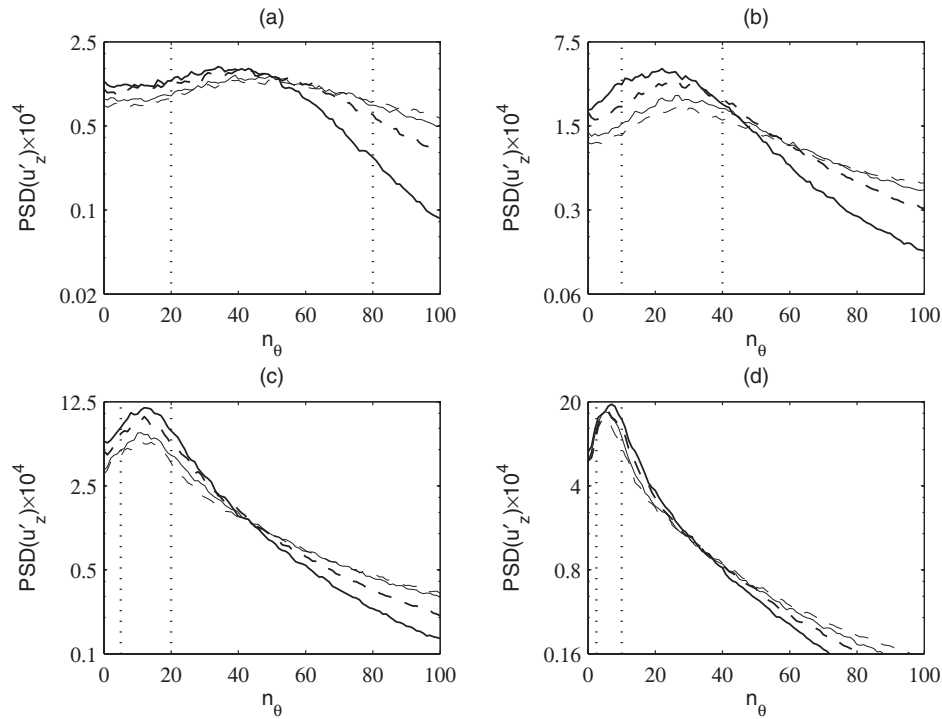
FIG. 14. Power spectral densities normalized by u_j of velocity u'_z as functions of azimuthal mode n_θ, at $r = r_0$ at the axial positions (a) $z = 0.4r_0$, (b) where $\delta_\theta = 0.036r_0$, (c) where $\delta_\theta = 0.072r_0$, and (d) where $\delta_\theta = 0.144r_0$: (bold solid) JetRe25e3, (bold dashed) JetRe50e3, (thin solid) JetRe100e3, (thin dashed) JetRe200e3. The dotted lines indicate approximately $\lambda_\theta = 2\delta$ and $\delta/2$, from left to right.

do not depend much on the Reynolds number, which agrees with the present trends. In this study, an instability-like component therefore emerges initially in the highly disturbed shear layers, which is attributed to the facts that the exit boundary layers are transitional but not fully turbulent, and that the Reynolds numbers are moderate. This component can indeed be seen very distinctly at $\mathrm{Re}_D = 2.5 \times 10^4$ (and $\mathrm{Re}_\theta = 256$), but to a lesser extent with increasing Re_D, which also raises the question of its possible disappearance in high-Reynolds-number jets typically for $\mathrm{Re}_\theta \geq 5000$ and $\mathrm{Re}_D \geq 5 \times 10^5$.

To track the evolution of the frequencies dominating in the shear layers, the peak Strouhal numbers in the spectra of u'_r at $r = r_0$ are represented in Figure 13(b). In all cases, a gradual decrease is observed with the axial distance, as the mixing layers spread. At $\mathrm{Re}_D = 2.5 \times 10^4$, values around the peak Strouhal number $\mathrm{St}_D = 1.4$ noticed at $z = r_0$ are found over a non-negligible axial extent, approximately between $z = 0.5r_0$ and $z = 2r_0$. This suggests the presence of large-scale structures just downstream of the nozzle. In this case, and in the others, there is however no clear step from $\mathrm{St}_D = 1.4$ down to its subharmonic $\mathrm{St}_D = 0.7$, as occurs in initially laminar jets around the first stage of vortex pairings.[37,38] Based on the velocity spectra, the presence of pairings of large-scale vortical structures in the present initially highly disturbed jets is therefore difficult to demonstrate.

Azimuthal spectra of the fluctuating axial velocity are calculated at four positions on the lip line, and represented as a function of the azimuthal mode n_θ in Figure 14 using a linear scale for the x-axis. The first position is $z = 0.4r_0$ as previously in Figures 3(b) and 4(b). The second one is between $z = 0.9r_0$ and $z = r_0$ depending on Re_D, and corresponds to the location where the shear-layer momentum thickness δ_θ is equal to $0.036r_0$, which is about twice the value of $\delta_\theta(0)$ at the nozzle exit. Similarly, the two final positions are obtained between $z = 2.1r_0$ and $z = 3r_0$, and between $z = 4.5r_0$ and $z = 6.2r_0$, for $\delta_\theta = 0.072r_0 \simeq 4\delta_\theta(0)$ and $\delta_\theta = 0.144r_0 \simeq 8\delta_\theta(0)$, respectively. The different positions are illustrated in Figure 10(a) using dotted lines and in Figure 16 using circles. The shear-layer thickness δ at these positions is naturally assumed to be δ_0, $2\delta_0$, $4\delta_0$, and $8\delta_0$, where δ_0 is the inlet boundary-layer thickness, to determine the modes n_θ for which the azimuthal wave
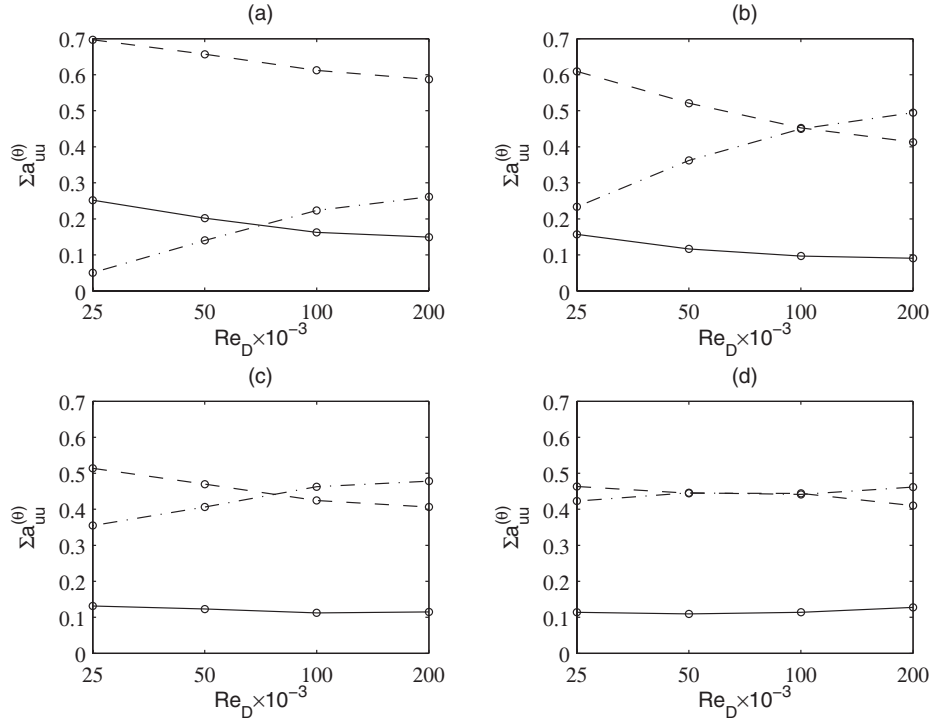
FIG. 15. Variations with Re_D of the truncated sums of coefficients $a_{uu}^{(\theta)}$ obtained from functions $\mathcal{R}_{uu}^{(\theta)}$ at $r = r_0$ at the axial positions (a) $z = 0.4r_0$, (b) where $\delta_\theta = 0.036r_0$, (c) where $\delta_\theta = 0.072r_0$, and (d) where $\delta_\theta = 0.144r_0$: (solid) $a_{uu}^{(\theta)}|_{VLS}$, (dashed) $a_{uu}^{(\theta)}|_{LS}$, (dotted-dashed) $a_{uu}^{(\theta)}|_{FS}$, refer to expressions (2).

number λ_θ is equal to 2δ and $\delta/2$. The specific values thus found are represented as dotted lines in Figure 14, in the same way as in Figure 4(b). In all cases, the dominant azimuthal modes lie in the range of wave numbers $\delta/2 \leq \lambda_\theta \leq 2\delta$, with a peak around $\lambda_\theta \simeq \delta$. The broadening of the spectra with Re_D, leading to a strengthening of higher modes, is also apparent. It is however less marked as axial position increases.

The contributions of the very large, large, and fine-scale structures to the turbulent energy are finally estimated at the four positions defined above. As previously, they are, respectively, given by the three truncated sums of Fourier coefficients $a_{uu}^{(\theta)}$, obtained from the azimuthal correlation functions $\mathcal{R}_{uu}^{(\theta)}$ of velocity u'_z,

$$\begin{cases} a_{uu}^{(\theta)}|_{VLS} = \sum a_{uu}^{(\theta)}|_{\lambda_\theta \geq 2\delta}, \\ a_{uu}^{(\theta)}|_{LS} = \sum a_{uu}^{(\theta)}|_{\delta/2 \leq \lambda_\theta \leq 2\delta}, \\ a_{uu}^{(\theta)}|_{FS} = \sum a_{uu}^{(\theta)}|_{\lambda_\theta \leq \delta/2 \ \& \ n_\theta \leq 128}, \end{cases} \tag{2}$$

where δ is the local shear-layer thickness. They are displayed in Figure 15 as a function of Re_D. At $z = 0.4r_0$, as discussed in Sec. III A, most of the energy is contained in the large scales since $a_{uu}^{(\theta)}|_{LS} > 50\%$ in Figure 15(a) whatever the Reynolds number. The value of $a_{uu}^{(\theta)}|_{LS}$ decreases with Re_D, whereas that of $a_{uu}^{(\theta)}|_{FS}$ increases. At the other positions considered, the contribution of the scales such that $\delta/2 \leq \lambda_\theta \leq 2\delta$ remains greater than 40%, whereas that of larger scales does not exceed 15% in all cases. The contribution of the fine scales with azimuthal spacings smaller than $\delta/2$ however varies significantly. It grows with the local mixing-layer Reynolds number, which rises with both axial position and jet Reynolds number. Far from the nozzle exit, it becomes similar to the contribution of the large scales, and $a_{uu}^{(\theta)}|_{FS} \simeq a_{uu}^{(\theta)}|_{LS}$ is obtained. The latter condition is satisfied for $Re_D \geq 10^5$ in Figure 15(b), for $Re_D \geq 5 \times 10^4$ in Figure 15(c), and for $Re_D \geq 2.5 \times 10^4$ in Figure 15(d). In the present jets, the influence of the Reynolds number on the turbulent flow structure is consequently appreciable upstream of $z \simeq 5r_0$, but is relatively weak farther downstream.
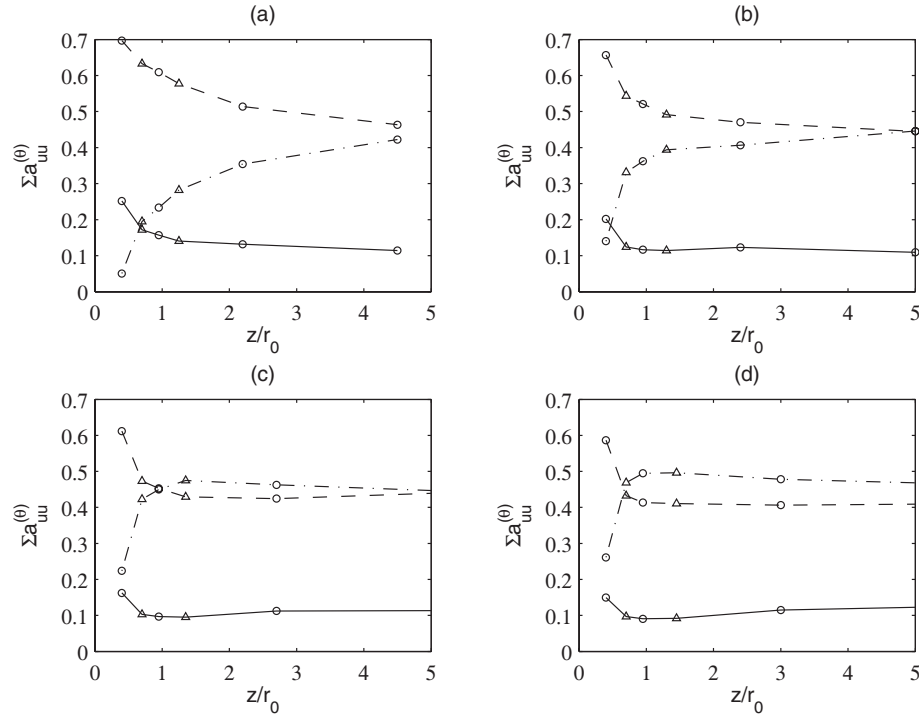
FIG. 16. Variations in (a) JetRe25e3, (b) JetRe50e3, (c) JetRe100e3, and (d) JetRe200e3 of the sums of coefficients $a_{uu}^{(\theta)}$ at $r = r_0$: (solid) $a_{uu}^{(\theta)}|_{VLS}$, (dashed) $a_{uu}^{(\theta)}|_{LS}$, (dotted-dashed) $a_{uu}^{(\theta)}|_{FS}$, refer to expressions (2). Results obtained: (circle) at $z = 0.4r_0$ and where $\delta_\theta = 0.036r_0$, $0.072r_0$ or $0.144r_0$, (triangle) where $\delta_\theta = 0.03r_0$ or $0.045r_0$.

In order to shed additional light on the decay of turbulent structures in the shear layers, the sums of Fourier coefficients $a_{uu}^{(\theta)}|_{VLS}$, $a_{uu}^{(\theta)}|_{LS}$, and $a_{uu}^{(\theta)}|_{FS}$ are represented in Figure 16 as a function of z/r_0. The values obtained at the four positions considered above and at the positions where $\delta_\theta = 0.03r_0$ or $0.045r_0$, yielding $z = 0.7r_0$ and $1.25r_0 \leq z \leq 1.45r_0$ respectively, are plotted. As also previously shown in Figure 15, the contribution of large scales is initially dominant and decreases with the axial position. The distance from the nozzle exit needed to reach $a_{uu}^{(\theta)}|_{FS} = a_{uu}^{(\theta)}|_{LS}$ is found to shorten strongly with the Reynolds number. It is, for instance, equal to $5r_0$ for $\mathrm{Re}_D = 5 \times 10^4$ in Figure 16(b), to r_0 for $\mathrm{Re}_D = 10^5$ in Figure 16(c), and to $0.7r_0$ for $\mathrm{Re}_D = 2 \times 10^5$ in Figure 16(d). Farther downstream, the truncated sums of coefficients do not vary significantly with z. The balance between large-scale and fine-scale contributions seems however to tilt in favor of the latter with increasing Reynolds number.

C. Jet flow development

Vorticity fields obtained up to $z = 25r_0$ in the four jets are represented in Figure 17 and in movie 2. They do not fundamentally differ, especially downstream of $z \simeq 10r_0$. In the jets at higher Reynolds numbers, the mixing layers appear however to begin to interact slightly farther downstream, in agreement with the reduction in shear-layer growth rate described in Sec. III B, which should result in longer potential cores.

The variations of the centerline mean axial velocity u_c and of the jet half-width $\delta_{0.5}$ are presented in Figures 18(a) and 18(b). With increasing Reynolds number, the velocity decay and the jet spreading both start at larger distances from the nozzle exit, leading to potential cores ending at $z_c = 13.8r_0$ in JetRe25e3, $z_c = 14.7r_0$ in JetRe50e3, and $z_c \simeq 15.8r_0$ in JetRe100e3 and JetRe200e3, where $u_c(z_c) = 0.95u_j$, as reported in Table V and illustrated in Figure 20(a). Downstream of the potential core, they appear similar regardless of Re_D, which is clearly demonstrated in Figure 21(a) where the mean axial velocity profiles, re-plotted as a function of $z - z_c$, nearly collapse. The influence of the Reynolds
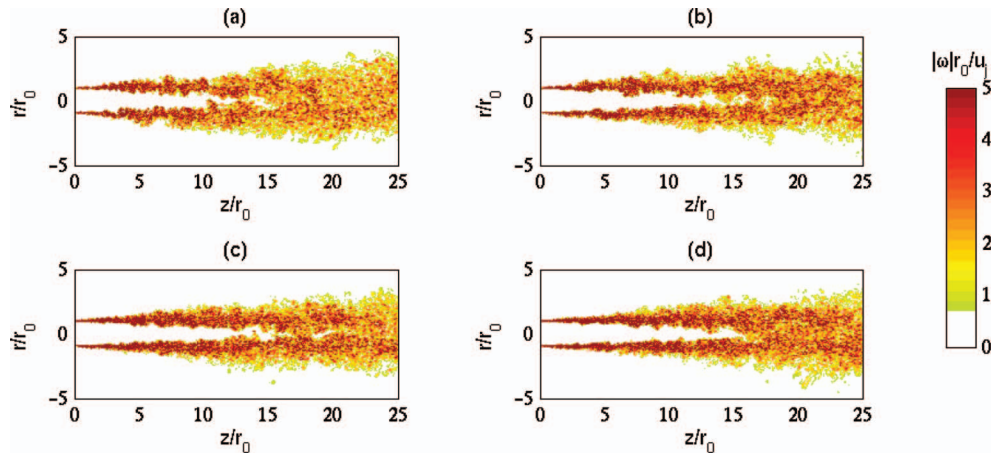
FIG. 17. Snapshots in the (z, r) plane of vorticity norm $|\boldsymbol{\omega}|$ in the jets: (a) JetRe25e3, (b) JetRe50e3, (c) JetRe100e3, (d) JetRe200e3 (enhanced online) [URL: http://dx.doi.org/10.1063/1.4757667.2].

number on the mean flow development is therefore relatively limited, and mainly consists of a shift in the axial direction. This behaviour is consistent with results of previous studies in which the Reynolds number dependence of the centerline velocity decay was found to be significant[8,9,11–13,44,45] for jets at Reynolds numbers lower than 10^4, but rather weak otherwise. Poor sensitivity was observed, for instance, in the experiments of Deo *et al.*[13] for plane jets at width-based $Re_h = 10^4$ and 1.65×10^4 (and $Re_\theta = 400$ and 643), and in those of Fellouah *et al.*[14] for round jets at $Re_D = 10^4$ and 3×10^4. Finally, in order to show comparisons with experimental data of the literature, measurements obtained by Lau *et al.*,[75] Arakeri *et al.*,[76] and Fleury *et al.*[71] for Mach number 0.9 round jets at $Re_D \geq 5 \times 10^5$ are depicted in Figure 18. Despite uncertainties regarding the jet nozzle-exit conditions, it can be noted that these data correspond well to the simulation results.

    The variations of the centerline rms values of axial and radial fluctuating velocities are displayed in Figures 19(a) and 19(b). With increasing Reynolds number, the maximum rms values are reached farther downstream, in agreement with the delay in mean flow field development, but they do not change much. As shown in Table V and in Figure 20(b), they are close to 12% of the jet velocity for u'_z and to 9.5% for u'_r in all cases. They are nevertheless slightly higher in the jet at $Re_D = 2.5 \times 10^4$, in accordance with a tendency appearing in experiments[13] and simulations[45] for low Reynolds numbers. When shifted in the axial direction with respect to the potential core length, as is the case in Figure 21(b) for the radial velocity component, the rms velocity profiles are moreover very similar.
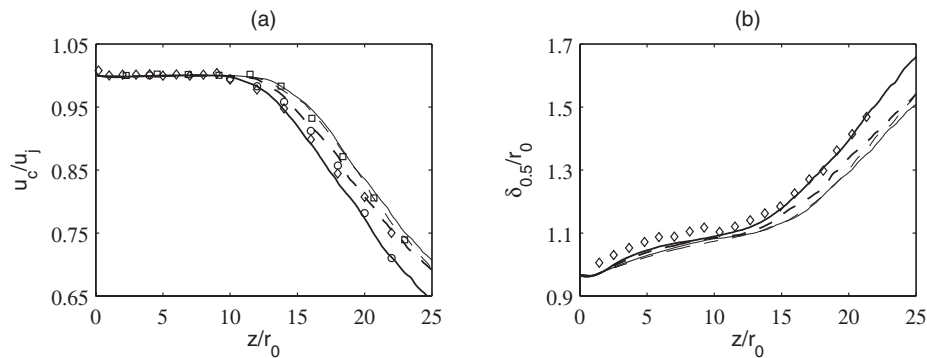

FIG. 18. Variations (a) of centerline mean axial velocity u_c and (b) of jet half-width $\delta_{0.5}$: (bold solid) JetRe25e3, (bold dashed) JetRe50e3, (thin solid) JetRe100e3, (thin dashed) JetRe200e3. Measurements for Mach 0.9 jets at $Re_D \geq 5 \times 10^5$: (circle) Lau *et al.*,[75] (square) Arakeri *et al.*,[76] (diamond) Fleury *et al.*[71]
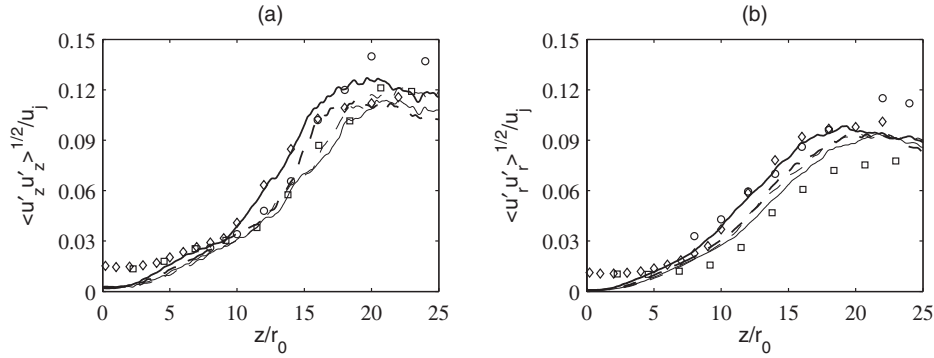
FIG. 19. Variations of centerline rms values of fluctuating velocities (a) u'_z and (b) u'_r: (bold solid) JetRe25e3, (bold dashed) JetRe50e3, (thin solid) JetRe100e3, (thin dashed) JetRe200e3. See caption of Figure 18 for the symbols.

Finally, it can be noticed that the present turbulence intensity profiles are roughly comparable to measurements available for Mach number 0.9 jets at $\mathrm{Re}_D \geq 5 \times 10^5$.

D. Acoustic fields

In order to provide a glimpse of the jet acoustic features, snapshots of the near-field fluctuating pressure obtained directly by LES are presented in Figure 22 and in movie 3. Significant differences can be observed in the sound fields. As the Reynolds number increases, the noise levels first appear to decrease. At a distance of $5r_0$ from the centerline, the peak values of pressure fluctuations between $z = 0$ and $z = 10r_0$ are, for instance, around 140 Pa in Figure 22(a) for the jet at $\mathrm{Re}_D = 2.5 \times 10^4$, whereas they are only around 60 Pa in Figure 22(d) for the jet at $\mathrm{Re}_D = 2 \times 10^5$. The structure of the sound fields also changes. For $\mathrm{Re}_D = 2.5 \times 10^4$ and 5×10^4, they display low-frequency acoustic waves emitted approximately between $z = 2.5r_0$ and $z = 5r_0$ during the early stages of shear-layer development, whereas they show a more complicated pattern for higher Reynolds numbers.

The jet far-field characteristics are examined from the pressure signals obtained at 60 radii from the nozzle exit using the wave extrapolation method documented in Sec. II D. The sound pressure levels determined at this distance are represented in Figure 23 for angles ϕ between $30°$ and $110°$ relative to the flow direction. Compared to measurements provided by Mollo-Christensen et al.,[32] Lush,[77] and Bogey et al.[78] for Mach number 0.9 jets at Reynolds numbers higher than $\mathrm{Re}_D = 5 \times 10^5$, they are found to be higher for all radiation angles. They however decrease with Re_D, which is not surprising given the lowering of peak turbulence intensities in Figure 11, reducing the gap with
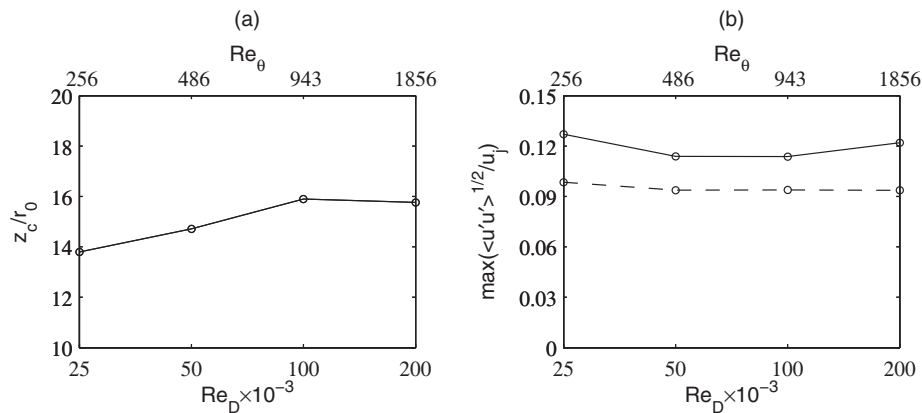

FIG. 20. Variations with Re_D and Re_θ (a) of the axial position of the end of the potential core z_c, and (b) of the peak rms values of velocities (solid) u'_z and (dashed) u'_r on the jet axis.
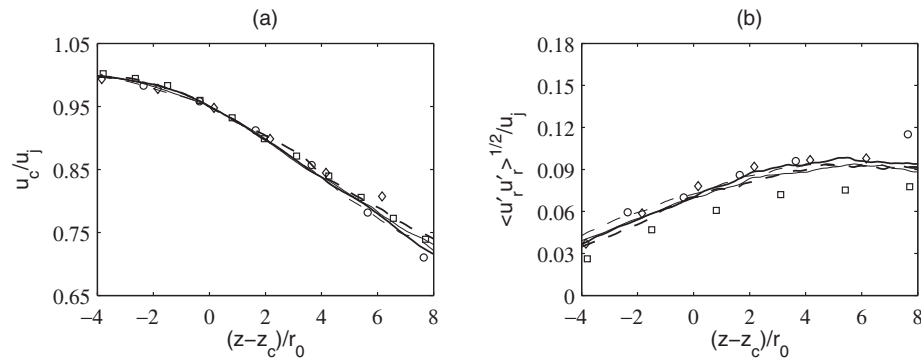
FIG. 21. Variations (a) of centerline mean axial velocity u_c, and (b) of centerline rms values of radial velocity u'_r, as a function of $(z - z_c)/r_0$: (bold solid) JetRe25e3, (bold dashed) JetRe50e3, (thin solid) JetRe100e3, (thin dashed) JetRe200e3. See caption of Figure 18 for the symbols.

respect to the experimental data. In the sideline direction at $\phi = 90°$, in particular, the simulations give values of 110.2 dB at $\mathrm{Re}_D = 2.5 \times 10^4$, 109.2 dB at $\mathrm{Re}_D = 5 \times 10^4$, and 108 dB at $\mathrm{Re}_D = 10^5$ and 2×10^5, whereas the measurements at $\mathrm{Re}_D \geq 5 \times 10^5$ range from 105.8 to 106.8 dB.

Similar variations of the sound levels with the Reynolds number are shown by results of the literature. Indeed, if an increase of the Reynolds number leads to stronger noise for initially laminar free shear flows at low Reynolds numbers, namely jets[31,42,46] at $\mathrm{Re}_D \leq 10^4$ and mixing layers[47] at $\mathrm{Re}_\theta \leq 500$, noise reduction arose in a few experiments on circular jets at moderate Reynolds numbers as in this study. This trend was, for instance, identified by Viswanathan[36] for hot jets at $\mathrm{Re}_D \leq 4 \times 10^5$. It seems also, and especially, to apply to the tripped jets of Zaman[15] at $\mathrm{Re}_D \leq 2 \times 10^5$, for
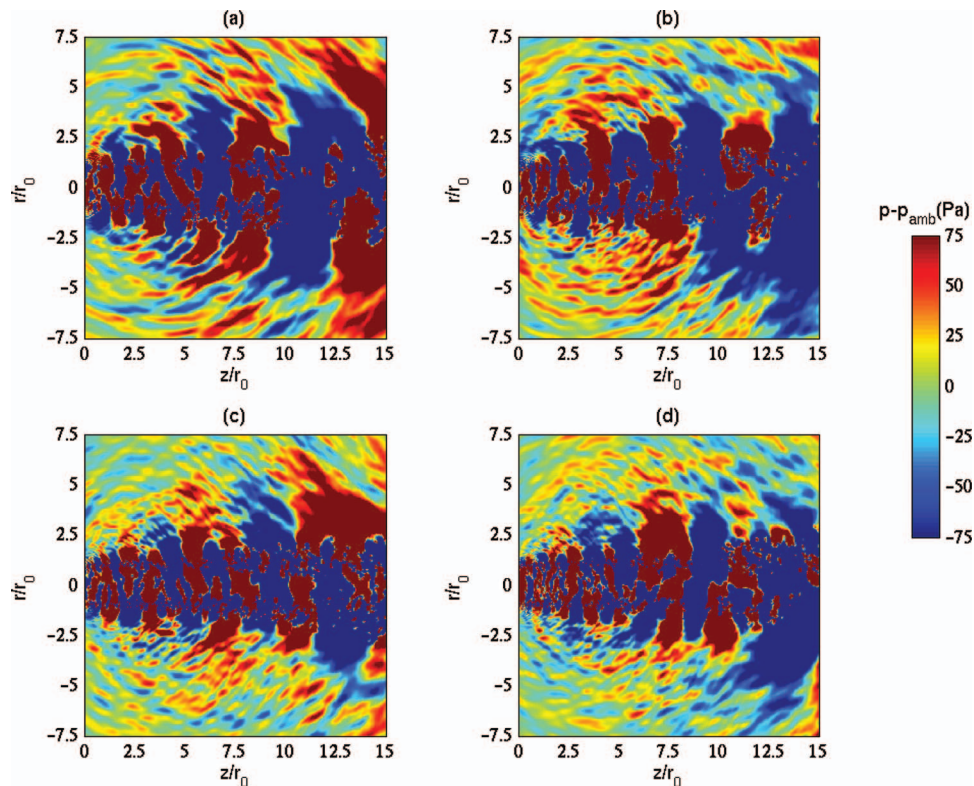

FIG. 22. Snapshots in the (z, r) plane of fluctuating pressure $p - p_a$ obtained in: (a) JetRe25e3, (b) JetRe50e3, (c) JetRe100e3, (d) JetRe200e3 (enhanced online) [URL: http://dx.doi.org/10.1063/1.4757667.3].

TABLE V. Axial position of the end of the potential core z_c, and peak rms values of fluctuating velocities u'_z and u'_r on the jet axis.

	z_c/r_0	$\langle u'^2_z \rangle^{1/2}/u_j$	$\langle u'^2_r \rangle^{1/2}/u_j$
JetRe25e3	13.8	12.7%	9.8%
JetRe50e3	14.7	11.4%	9.4%
JetRe100e3	15.9	11.4%	9.4%
JetRe200e3	15.8	12.2%	9.4%

which the nozzle-exit parameters $\delta_\theta(0)/r_0 \simeq 0.018$ and $u'_e/u_j \simeq 0.09$ were nearly constant and similar to those in the present jets. This is suggested by the fact that, with decreasing Reynolds number, the sound levels of Zaman's jets rose above the levels extrapolated from high-Reynolds-number data using the usual jet velocity power laws. The discrepancy is, for instance, of the order of 3 dB at $Re_D = 1.3 \times 10^5$, see Figure 3 in Zaman's paper,[15] which is consistent with the simulation results. Lowering the Reynolds number of initially highly disturbed jets at moderate Re_D consequently increases the sound levels with respect to the asymptotically lower levels observed for high Reynolds numbers. The jets most probably generate additional noise components resulting from the evolution of more intense large-scale structures in the shear layers as described in Sec. III B, which is discussed below based on sound spectra.

The pressure spectra obtained at $60r_0$ from the nozzle exit at the angles $\phi = 30°, 40°, 60°,$ and $90°$ relative to the jet direction are represented in Figure 24, together with measurements of Tanna[79] and Bogey *et al.*[78] for Mach number 0.9 jets at $Re_D \geq 7.8 \times 10^5$. The Strouhal number $St_D = 0.7$, which is half the frequency predominant at $z = r_0$ in the shear layers as shown in Figure 13(a), is also drawn. With increasing Reynolds number, as noticed previously for the far-field directivity, the noise levels decrease by about 2 dB over the Re_D range considered, yielding spectra progressively closer to the experimental spectra at the four radiation angles.

At $\phi = 30°$ and $40°$, in Figures 24(a) and 24(b), noise reduction is significant for $St_D \geq 0.5$, but rather limited for lower Strouhal numbers. The jet noise components around $St_D = 0.15$ dominating in the downstream direction therefore turn out to be weakly sensitive to Reynolds number, as found in previous numerical studies.[46] At $\phi = 90°$, in Figure 24(d), the sound levels are on the contrary reduced for all frequencies. The strong acoustic components observed for $St_D \leq 0.5$ for JetRe25e3 and JetRe50e3, as is the case in the sideline spectra obtained by Viswanathan[36] for hot jets at similar Reynolds numbers, are attenuated, leading to a good agreement with the measurements for JetRe100e3 and JetRe200e3 for lower frequencies. The components for $St_D \geq 0.5$ are also damped, but there remains a slight overestimation by 2–3 dB with respect to the experimental data for the higher Reynolds number jets, as for the tripped jets of Zaman[15] with comparable nozzle-exit conditions. As also argued in recent papers,[38,49] this can be attributed to the persistence of large-scale
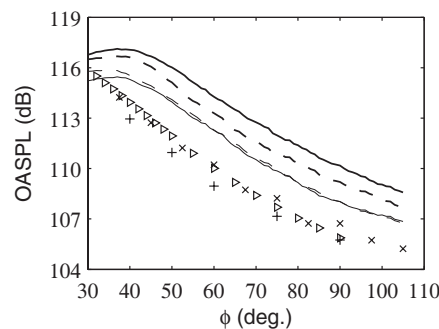

FIG. 23. Overall sound pressure levels at $60r_0$ from the nozzle exit, as a function of the angle ϕ relative to the jet direction: (bold solid) JetRe25e3, (bold dashed) JetRe50e3, (thin solid) JetRe100e3, (thin dashed) JetRe200e3. Measurements for jets at $Re_D \geq 5 \times 10^5$: (plus) Mollo-Christensen *et al.*,[32] (times) Lush,[77] (right-pointing triangle) Bogey *et al.*[78]
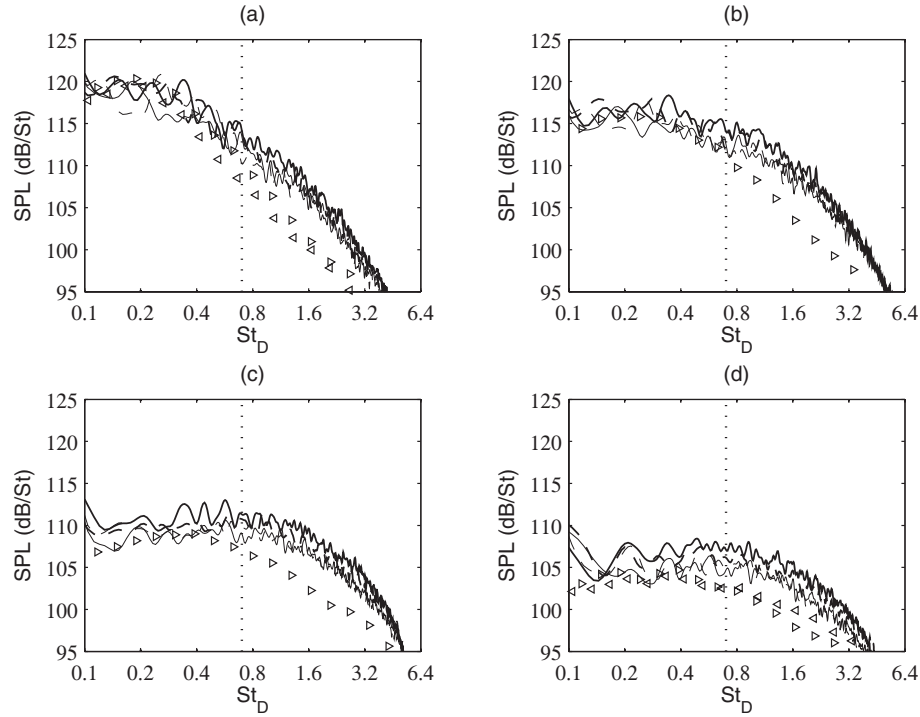
FIG. 24. Sound pressure levels at $60r_0$ from the nozzle exit, as a function of St_D, at the angles ϕ of (a) 30°, (b) 40°, (c) 60° and (d) 90°: (bold solid) JetRe25e3, (bold dashed) JetRe50e3, (thin solid) JetRe100e3, (thin dashed) JetRe200e3. The dotted lines indicate $St_D = 0.7$. Measurements for jets at $Re_D \geq 7.8 \times 10^5$: (left-pointing triangle) Tanna,[79] (right-pointing triangle) Bogey *et al.*[78]

vortical structures in the present jets, whose moderate Reynolds numbers $Re_D \simeq 10^5$ are about one order of magnitude lower than the values usually encountered in experiments. Note finally that the additional noise components radiated by the jets are roughly centered, especially at $\phi = 90°$, around the Strouhal number value of $St_D = 0.7$ which is expected if there is a first stage of vortex pairings downstream of the nozzle in the present jets. This further supports the fact that these components are generated by the interactions of large-scale structures in the shear layers.

IV. CONCLUSION

In this paper, the effects of moderate Reynolds numbers on the flow and sound fields of initially highly disturbed round jets at Mach number 0.9 have been investigated under well controlled conditions. For nozzle-exit boundary-layer parameters $H \simeq 2.3$, $\delta_\theta(0)/r_0 \simeq 0.018$ and $u'_e/u_j \simeq 0.09$, these effects have been found to be significant for the ranges of diameter and momentum-thickness Reynolds numbers $2.5 \times 10^4 \leq Re_D \leq 2 \times 10^5$ and $256 \leq Re_\theta \leq 1856$ considered. To summarize the most important changes, jets at higher Reynolds numbers show mixing layers developing more slowly with lower turbulence intensities, have a slightly longer potential core, and produce less noise. These results are attributed to the weakening of the large-scale structures, and consequently of their interactions, and to the strengthening of the fine-scale structures, which have been observed in the shear layers as Re_D and Re_θ increase. They naturally raise the question of the threshold values of Re_D and Re_θ above which Reynolds number independence is reached. This could be studied in the future by computing jets typically at $Re_D \geq 5 \times 10^5$, using many more grid points than in this work to properly deal with such high Reynolds number values.

The effects of higher Reynolds numbers on jet flow and acoustic features are similar to those obtained by increasing the levels of nozzle-exit velocity disturbances.[38] Therefore, they can mutually amplify or, on the contrary, they can oppose one another when the Reynolds numbers and the exit

turbulence intensities vary following opposite trends. The latter situation seems to have occurred, for instance, in a recent experiment by Zaman[17] for two jets exhausting from nozzles of same diameter but different geometries: using the so-called conic nozzle, the ratio $\delta_\theta(0)/r_0$, hence Re_θ, increased, whereas u'_e/u_j decreased at the nozzle exit. In such cases, it may be difficult to know *a priori* the way in which the jet properties will vary. Finally, as mentioned above for Zaman's experiment, in jets at identical diameter and Reynolds number Re_D, the Reynolds numbers Re_θ are likely to differ depending on the exit boundary-layer thickness. As a result, the latter parameter is important in jets for several reasons. Its influence on initially highly disturbed jets at moderate Reynolds numbers has been examined in a recent study.[80]

ACKNOWLEDGMENTS

[1] H. Sato, "The stability and transition of a two-dimensional jet," J. Fluid Mech. **7**(1), 53 (1964).

[2] E. Mollö-Christensen and R. Narasimha, "Sound emission from jets at high subsonic velocities," J. Fluid Mech. **8**(1), 49 (1960).

[3] D. G. Crighton, "Acoustics as a branch of fluid mechanics," J. Fluid Mech. **106**, 261 (1981).

[4] A. K. M. F. Hussain, "Coherent structures–reality and myth," Phys. Fluids **26**(10), 2816 (1983).

[5] P. J. Morris, "The spatial viscous instability of axisymmetric jets," J. Fluid Mech. **77**(3), 511 (1976).

[6] P. J. Morris, "Viscous stability of compressible axisymmetric jets," AIAA J. **21**(4), 481 (1983).

[7] A. Michalke, "Survey on jet instability theory," Prog. Aerosp. Sci. **21**, 159 (1984).

[8] G. P. Lemieux and P. H. Oosthuizen, "Experimental study of the behaviour of plane turbulent jets at low Reynolds numbers," AIAA Paper No. 84-1661, 1984; AIAA J. **23**(12), 1845 (1985).

[9] I. Namer and M. V. Ötügen, "Velocity measurements in a plane turbulent air jet at moderate Reynolds numbers," Exp. Fluids **6**, 387 (1988).

[10] T. H. Weisgraber and D. Liepmann, "Turbulent structure during transition to self-similarity in a round jet," Exp. Fluids **14**, 210 (1998).

[11] G. Papadopoulos and W. M. Pitts, "Scaling the near-field centerline mixing behavior of axisymmetric turbulent jets," AIAA J. **36**(9), 1635 (1998).

[12] S. J. Kwon and I. W. Seo, "Reynolds number effects on the behavior of a non-buoyant round jet," Exp. Fluids **38**(6), 801 (2005).

[13] R. C. Deo, J. Mi, and G. J. Nathan, "The influence of Reynolds number on a plane jet," Phys. Fluids **20**(1), 075108 (2008).

[14] H. Fellouah, C. G. Ball, and A. Pollard, "Reynolds number effects within the development region of a turbulent round jet," Int. J. Heat Mass Transfer **52**, 3943 (2009).

[15] K. B. M. Q. Zaman, "Effect of the initial condition on subsonic jet noise," AIAA J. **23**(9), 1370 (1985).

[16] K. B. M. Q. Zaman, "Far-field noise of a subsonic jet under controlled excitation," J. Fluid Mech. **152**, 83 (1985).

[17] K. B. M. Q. Zaman, "Effect of initial boundary-layer state on subsonic jet noise," AIAA J. **50**(8), 1784 (2012).

[18] A. K. M. F. Hussain and M. F. Zedan, "Effects of the initial condition on the axisymmetric free shear layer: Effects of the initial momentum thickness," Phys. Fluids **21**(7), 1100 (1978).

[19] A. K. M. F. Hussain and M. F. Zedan, "Effects of the initial condition on the axisymmetric free shear layer: Effects of the initial fluctuation level," Phys. Fluids **21**(9), 1475 (1978).

[20] E. Gutmark and C.-M. Ho, "Preferred modes and the spreading rates of jets," Phys. Fluids **26**(10), 2932 (1983).

[21] S. C. Crow and F. H. Champagne, "Orderly structure in jet turbulence," J. Fluid Mech. **48**, 547 (1971).

[22] G. L. Brown and A. Roshko, "Density effect and large structure in turbulent mixing layers," J. Fluid Mech. **64**, 775 (1974).

[23] C. Chandrsuda, R. D. Mehta, A. D. Weir, and P. Bradshaw, "Effect of free stream turbulence on large structure in turbulent mixing layer," J. Fluid Mech. **85**(4), 693 (1978).

[24] I. Wygnanski, D. Oster, H. Fiedler, and B. Dziomba, "On the perseverance of a quasi-two-dimensional eddy-structure in a turbulent mixing layer," J. Fluid Mech. **93**(2), 325 (1979).

[25] F. K. Browand and B. O. Latigo, "Growth of the two-dimensional mixing layer from a turbulent and nonturbulent boundary layer," Phys. Fluids **22**(6), 1011 (1979).

[26] K. B. M. Q. Zaman and A. K. M. F. Hussain, "Vortex pairing in a circular jet under controlled excitation. Part 1. General jet response," J. Fluid Mech. **101**(3), 449 (1980).

[27] K. B. M. Q. Zaman and A. K. M. F. Hussain, "Natural large-scale structures in the axisymmetric mixing layer," J. Fluid Mech. **138**, 325 (1984).

[28] C. K. W. Tam, "Supersonic jet noise," Annu. Rev. Fluid Mech. **27**, 17 (1995).

[29] G. L. Morrison and D. K. McLaughlin, "Noise generation by instabilities in low Reynolds number supersonic jets," J. Sound Vib. **65**(2), 177 (1979).

[30] T. R. Troutt and D. K. McLaughlin, "Experiments on the flow and acoustic properties of a moderate-Reynolds-number supersonic jet," J. Fluid Mech. **116**, 123 (1982).

[31] J. L. Stromberg, D. K. McLaughlin, and T. R. Troutt, "Flow field and acoustic properties of a Mach number 0.9 jet at a low Reynolds number," J. Sound Vib. **72**(2), 159 (1980).

[32] E. Mollo-Christensen, M. A. Kolpin, and J. R. Martucelli, "Experiments on jet flows and jet noise far-field spectra and directivity patterns," J. Fluid Mech. **18**, 285 (1964).

[33] K. Yamamoto and R. E. A. Arndt, "Peak Strouhal frequency of subsonic jet noise as a function of Reynolds number," AIAA Paper No. 79-1525, 1979.

[34] D. F. Long and R. E. A. Arndt, "Jet noise at low Reynolds number," AIAA J. **22**(2), 187 (1984).

[35] J. E. Bridges and A. K. M. F. Hussain, "Roles of initial conditions and vortex pairing in jet noise," J. Sound Vib. **117**(2), 289 (1987).

[36] K. Viswanathan, "Aeroacoustics of hot jets," J. Fluid Mech. **516**, 39 (2004).

[37] C. Bogey and C. Bailly, "Influence of nozzle-exit boundary-layer conditions on the flow and acoustic fields of initially laminar jets," J. Fluid Mech. **663**, 507 (2010).

[38] C. Bogey, O. Marsden, and C. Bailly, "Influence of initial turbulence level on the flow and sound fields of a subsonic jet at a diameter-based Reynolds number of 10^5," J. Fluid Mech. **701**, 352 (2012).

[39] T. Colonius and S. K. Lele, "Computational aeroacoustics: progress on nonlinear problems of sound generation," Prog. Aerosp. Sci. **40**, 345 (2004).

[40] C. Bailly and C. Bogey, "Contributions of CAA to jet noise research and prediction," Int. J. Comput. Fluid Dyn. **18**(6), 481 (2004).

[41] M. Wang, J. B. Freund, and S. K. Lele, "Computational prediction of flow-generated sound," Annu. Rev. Fluid. Mech. **38**, 483 (2006).

[42] J. B. Freund, "Noise sources in a low-Reynolds-number turbulent jet at Mach 0.9," J. Fluid Mech. **438**, 277 (2001).

[43] C. Bogey, C. Bailly, and D. Juvé, "Noise investigation of a high subsonic, moderate Reynolds number jet using a compressible LES," Theor. Comput. Fluid Dyn. **16**(4), 273 (2003).

[44] M. Klein, A. Sadiki, and J. Janicka, "Investigation of the influence of the Reynolds number on a plane jet using direct numerical simulation," Int. J. Heat Fluid Flow **24**, 785 (2003).

[45] C. Bogey and C. Bailly, "Large eddy simulations of transitional round jets: Influence of the Reynolds number on flow development and energy dissipation," Phys. Fluids **18**(6), 065101 (2006).

[46] C. Bogey and C. Bailly, "Investigation of downstream and sideline subsonic jet noise using large eddy simulations," Theor. Comput. Fluid Dyn. **20**(1), 23 (2006).

[47] R. R. Kleinman and J. B. Freund, "The sound from mixing layers simulated with different ranges of turbulent scales," Phys. Fluids **20**(10), 101503 (2008).

[48] J. Kim and H. Choi, "Large eddy simulation of a circular jet: effect of inflow conditions on the near field," J. Fluid Mech. **620**, 383 (2009).

[49] C. Bogey, O. Marsden, and C. Bailly, "Large-eddy simulation of the flow and acoustic fields of a Reynolds number 10^5 subsonic jet with tripped exit boundary layers," Phys. Fluids **23**(3), 035104 (2011).

[50] C. Bogey, O. Marsden, and C. Bailly, "On the spectra of nozzle-exit velocity disturbances in initially nominally turbulent jets," Phys. Fluids **23**(9), 091702 (2011).

[51] K. Mohseni and T. Colonius, "Numerical treatment of polar coordinate singularities," J. Comput. Phys. **157**(2), 787 (2000).

[52] C. Bogey, N. de Cacqueray, and C. Bailly, "Finite differences for coarse azimuthal discretization and for reduction of effective resolution near origin of cylindrical flow equations," J. Comput. Phys. **230**(4), 1134 (2011).

[53] C. Bogey and C. Bailly, "A family of low dispersive and low dissipative explicit schemes for flow and noise computations," J. Comput. Phys. **194**(1), 194 (2004).

[54] C. Bogey, N. de Cacqueray, and C. Bailly, "A shock-capturing methodology based on adaptative spatial filtering for high-order non-linear computations," J. Comput. Phys. **228**(5), 1447 (2009).

[55] J. Berland, C. Bogey, O. Marsden, and C. Bailly, "High-order, low dispersive and low dissipative explicit schemes for multiple-scale and boundary problems," J. Comput. Phys. **224**(2), 637 (2007).

[56] C. K. W. Tam and Z. Dong, "Radiation and outflow boundary conditions for direct computation of acoustic and flow disturbances in a nonuniform mean flow," J. Comput. Acoust. **4**(2), 175 (1996).

[57] C. Bogey and C. Bailly, "Three-dimensional non-reflective boundary conditions for acoustic simulations: far-field formulation and validation test cases," Acta Acustica united with Acustica **88**(4), 463 (2002).

[58] C. Bogey and C. Bailly, "Large eddy simulations of round free jets using explicit filtering with/without dynamic Smagorinsky model," Int. J. Heat Fluid Flow **27**(4), 603 (2006).

[59] C. Bogey and C. Bailly, "Turbulence and energy budget in a self-preserving round jet: direct evaluation using large-eddy simulation," J. Fluid Mech. **627**, 129 (2009).

[60] C. Bogey, S. Barré, D. Juvé, and C. Bailly, "Simulation of a hot coaxial jet: Direct noise prediction and flow-acoustics correlations," Phys. Fluids **21**(3), 035105 (2009).

[61] K. K. Ahuja, B. J. Tester, and H. K. Tanna, "Calculation of far field jet noise spectra from near field measurements with true source location," J. Sound Vib. **116**(3), 415 (1987).

[62] J. G. M. Eggels, F. Unger, M. H. Weiss, J. Westerweel, R. J. Adrian, R. Friedrich, and F. T. M. Nieuwstadt, "Fully developed turbulent pipe flow: a comparison between direct numerical simulation and experiment," J. Fluid Mech. **268**, 175 (1994).

[63] C. D. Tomkins and R. J. Adrian, "Energetic spanwise modes in the logarithmic layer of a turbulent boundary layer," J. Fluid Mech. **545**, 141 (2005).

[64] J. P. Monty, N. Hutchins, H. C. H. Ng, I. Marusic, and M. S. Chong, "A comparison of turbulent pipe, channel and boundary layer flows," J. Fluid Mech. **632**, 431 (2009).

[65] J. Jiménez, S. Hoyas, M. P. Simens, and Y. Mizuno, "Turbulent boundary layers and channels at moderate Reynolds numbers," J. Fluid Mech. **657**, 335 (2010).

[66] S. Ghosh, H. Foysi, and R. Friedrich, "Compressible turbulent channel and pipe flow: similarities and differences," J. Fluid Mech. **648**, 155 (2010).

[67] C. D. Tomkins and R. J. Adrian, "Spanwise structure and scale growth in turbulent boundary layers," J. Fluid Mech. **490**, 37 (2003).

[68] P. O. A. L. Davies, M. J. Fisher, and M. J. Barratt, "The characteristics of the turbulence in the mixing region of a round jet," J. Fluid Mech. **15**, 337 (1963).

[69] B. G. Jones, H. P. Planchon, and R. J. Hammersley, "Turbulent correlation measurements in a two-stream mixing layer," AIAA J. **11**(8), 1146 (1973).

[70] F. K. Browand and C. D. Troutt, "A note on spanwise structure in the two-dimensional mixing layer," J. Fluid Mech. **97**(4), 771 (1980).

[71] V. Fleury, C. Bailly, E. Jondeau, M. Michard, and D. Juvé, "Space-time correlations in two subsonic jets using dual-PIV measurements," AIAA J. **46**(10), 2498 (2008).

[72] P. J. Morris and K. B. M. Q. Zaman, "Velocity measurements in jets with application to noise source modelling," J. Sound Vib. **329**(4), 394 (2009).

[73] Z. D. Husain and A. K. M. F. Hussain, "Axisymmetric mixing layer: influence of the initial and boundary conditions," AIAA J. **17**(1), 48 (1979).

[74] R. E. Drubka, P. Reisenthel, and H. M. Nagib, "The dynamics of low initial disturbance turbulent jets," Phys. Fluids A **1**(10), 1723 (1989).

[75] J. C. Lau, P. J. Morris, and M. J. Fisher, "Measurements in subsonic and supersonic free jets using a laser velocimeter," J. Fluid Mech. **93**(1), 1 (1979).

[76] V. H. Arakeri, A. Krothapalli, V. Siddavaram, M. B. Alkislar, and L. Lourenco, "On the use of microjets to suppress turbulence in a Mach 0.9 axisymmetric jet," J. Fluid Mech. **490**, 75 (2003).

[77] P. A. Lush, "Measurements of subsonic jet noise and comparison with theory," J. Fluid Mech. **46**(3), 477 (1971).

[78] C. Bogey, S. Barré, V. Fleury, C. Bailly, and D. Juvé, "Experimental study of the spectral properties of near-field and far-field jet noise," Int. J. Aeroacoust. **6**(2), 73 (2007).

[79] H. K. Tanna, "An experimental study of jet noise. Part I: Turbulent mixing noise," J. Sound Vib. **50**(3), 405 (1977).

[80] C. Bogey, O. Marsden, and C. Bailly, "Effects of initial shear-layer thickness on turbulent subsonic jets at moderate Reynolds numbers," AIAA Paper No. 2012-2249, 2012.